

THE STRUCTURE AND REACTIVITY OF  
DOUBLY CHARGED IONS

A THESIS

Presented to

The Faculty of the Division of Graduate Studies

By

Jeffrey Hamilton Agee

In Partial Fulfillment  
of the Requirements for the Degree  
Master of Science in Chemistry

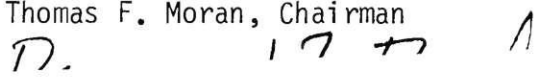
Georgia Institute of Technology

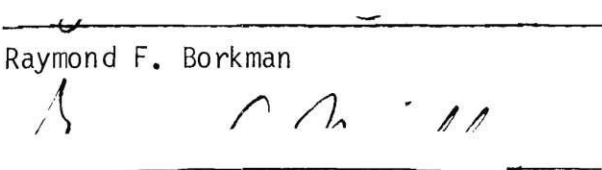
December, 1978

THE STRUCTURE AND REACTIVITY OF  
DOUBLY CHARGED IONS

Approved:

  
\_\_\_\_\_  
Thomas F. Moran, Chairman

  
\_\_\_\_\_  
Raymond F. Borkman

  
\_\_\_\_\_  
George A. Miller

Date approved by Chairman

Nov. 16, 1978

## ACKNOWLEDGMENTS

I would like to express my deepest gratitude to Dr. T.F. Moran, whose assistance and guidance as director of this project has ensured its success. In addition, the cooperation of Larry Abbey and John Wilcox has allowed this study to be completed with both speed and efficiency. Appreciation is also expressed to Dr. R.F. Borkman and Dr. G.A. Miller for reading this thesis. The tedious task of typing this manuscript was handled beautifully by Pat Cooke.

## TABLE OF CONTENTS

	Page
ACKNOWLEDGMENTS . . . . .	ii
LIST OF TABLES . . . . .	iv
LIST OF ILLUSTRATIONS . . . . .	v
SUMMARY . . . . .	vii
CHAPTER	
I. INTRODUCTION . . . . .	1
II. APPARATUS . . . . .	3
General Magnetic, Double Focusing Mass Spectrometer Time-of-Flight Mass Spectrometer	
III. POTENTIAL ENERGY CURVES . . . . .	18
IV. IONIZATION POTENTIALS . . . . .	28
Introduction Theory Experimental Results	
V. WAVEFUNCTION OVERLAP . . . . .	45
Transition Probability Squares of Overlap Integrals	
VI. RECOMBINATION ENERGY . . . . .	53
VII. REACTION CROSS SECTIONS . . . . .	58
Calculations	
VIII. CONCLUSIONS . . . . .	63
LITERATURE CITED . . . . .	65

## LIST OF TABLES

TABLE	Page
1. Spectroscopic Constants for States of $N_2^{++}$ , $O_2^{++}$ and $NO^{++}$ . . . . .	23
2. Appearance Potentials Obtained from Product Ion Efficiency Curves Analysis . . . . .	39
3. Summary of Ground State Ionization Potentials for $CO^{++}$ , $N_2^{++}$ , $NO^{++}$ and $O_2^{++}$ . . . . .	40
4. Relative Energies of $O_2^{++}$ Molecular Ion in eV . . . . .	42
5. Relative Energies of $N_2^{++}$ Molecular Ion in eV . . . . .	43
6. Relative Energies of $NO^{++}$ Molecular Ion in eV . . . . .	44
7. Squares of Overlap Integrals for the Ground $N_2(X^1\Sigma_g^-, v'' = 0)$ State with Vibrational Levels $v'$ of $N_2^{++}$ . . . . .	49
8. Squares of Overlap Integrals for the Ground $O_2(X^3\Sigma_g^-, v'' = 0)$ State with Vibrational Levels $v'$ of $O_2^{++}$ . . . . .	50
9. Relative Franck-Condon Factors for $CO^{++}(X^3\Pi, v'' = 0)$ . . . . .	51
10. Squares of Overlap Integrals for the Ground $NO(X^2\Pi, v'' = 0)$ State with Vibrational Levels $v'$ of $NO^{++}$ . . . . .	52
11. Cross Sections in the Range 1000-3000 eV for Reactions of the Type $N_2^{++} + AB \rightarrow N_2^+ + AB^+$ . . . . .	60

## LIST OF ILLUSTRATIONS

Page

## FIGURE

1.	Schematic Diagram of Apparatus Used to Study Ionization Efficiency Curves . . . . .	4
2.	Potential Energy Curves of the Ground State of $O_2$ and the Excited States of $O_2^{++}$ , as Predicted by Hurley . . . . .	24
3.	Potential Energy Curves of the Ground State of $N_2$ and the Excited States of $N_2^{++}$ , as Predicted by Hurley . . . . .	25
4.	Potential Energy Curves of the Ground State of CO and the Excited States of $CO^{++}$ , as Predicted by Hurley . . . . .	26
5.	Potential Energy Curves of the Ground State of NO and the Excited States of $NO^{++}$ , as Predicted by Hurley . . . . .	27
6.	Ionization Efficiency Curves for Species Involved in the Reaction: $Ar^{++} + Ar \rightarrow Ar^+$ . . . . .	31
7.	Ionization Efficiency Curves for Species Involved in the Reaction: $N_2^{++} + N_2 \rightarrow N_2^+$ . . . . .	32
8.	Ionization Efficiency Curve of $CO^+$ Involved in the Reaction: $CO^{++} + CO \rightarrow CO^+$ . . . . .	33
9.	Ionization Efficiency Curves for Species Involved in the Reaction: $O_2^{++} + O_2 \rightarrow O_2^+$ . . . . .	34
10.	Ionization Efficiency Curves for Species Involved in the Reaction: $CO_2^{++} + CO_2 \rightarrow CO_2^+$ . . . . .	35
11.	Ionization Efficiency Curve for $NO^+$ Involved in the Reaction: $NO^{++} + NO \rightarrow NO^+$ . . . . .	36
12.	Ionization Efficiency Curves for Species Involved in the Reaction: $I^{++} + I_2 \rightarrow I^+$ . . . . .	37
13.	Ionization Efficiency Curve for $I_2^+$ Involved in the Reaction: $I_2^{++} + I_2 \rightarrow I_2^+$ . . . . .	38

## LIST OF ILLUSTRATIONS (continued)

	Page
FIGURE	
14. Relative Probability of Transition from $N_2^{++}$ Excited Ion States to Excited States of $N_2^+$ Producing a Particular Recombination Energy . . . . .	55
15. Relative Probability of Transitions from $N_2^{++}$ Excited Ion States to Excited States of $N_2^+$ Producing a Particular Recombination Energy . . . . .	56
16. Recombination Energy of $N_2^+$ Averaged Over the First Four Excited States and the Ionization Potentials of Various Target Molecules . . . . .	57

## SUMMARY

Ionization efficiency curves, obtained using a double focusing, magnetic mass spectrometer, are used to determine ionization potentials of doubly charged molecular ions. Reaction cross sections have been measured using a time-of-flight mass spectrometer.

Franck-Condon factors have been computed for the  $N_2 \rightarrow N_2^{++}$  system using Morse anharmonic wavefunctions. From these factors, the vibrational state distribution of  $N_2^{++}$  in these experiments has been determined for ions in the lowest three electronically excited states. Charge transfer reactions involving the formation of fast  $N_2^+$  from  $N_2^{++}$  ions colliding with AB are dependent on the reaction energetics and the vibrational overlaps in the  $N_2^{++} + AB \rightarrow N_2^+ + AB^+$  process. Transitions from  $N_2^{++}$  to  $N_2^+$  release energy which must balance that needed to ionize the target molecule AB. The reaction cross section for processes of this type is related to the range of recombination energies of the  $N_2^{++}$  ions in all excited states of  $N_2^{++}$  produced by electron impact.

The magnitude of the charge transfer cross sections involving  $N_2^{++}$  ions is correlated with the degree of vibrational overlap and the degree of energy balance between the  $N_2^{++} + AB$  reactants and the  $N_2^+ + AB^+$  products.

## CHAPTER I

## INTRODUCTION

When an electron interacts with a neutral molecule some doubly charged ions are formed. In the case of  $A_2$ , the following reactions are possible:



Subsequent interactions involving doubly charged ions formed in Equations (2) and (3) lead to the formation of a variety of species, several of which are shown below:



Mass spectrometers provide a means of distinguishing molecules with different mass to charge ratios,  $(m/e)$ . Ions with identical  $(m/e)$  values, such as  $A_2^{++}$  and  $A^+$ , are difficult to separate and as a result, molecular ions of the form  $A_2^{++}$  have received little study. Current

methods which have been applied to studies involving neutral and singly ionized molecules encounter severe problems when used in the study of doubly ionized molecules. These methods include emission spectroscopy, absorption spectroscopy, photoionization,<sup>1</sup> electron impact spectroscopy,<sup>2</sup> and photoelectron spectroscopy.<sup>3</sup>

The purpose of this work is to categorize the  $A_2^{++}$  and  $AB^{++}$  states and to use this knowledge in determining the reactivity of these double charged ions.

## CHAPTER II

### APPARATUS

#### General

A magnetic, double focusing mass spectrometer was used to measure ionization efficiency curves in these experiments. Reaction cross sections are more conveniently determined with a time-of-flight instrument. As will be pointed out, the 2E spectrum for the  $AB^+$  products of  $AB^{++} + M$  charge transfer reactions is free from any background contributions. Therefore, accurate ionization curves can be obtained for these ionic products.

#### Magnetic, Double Focusing Mass Spectrometer

##### Experimental

Reactant ions are produced in a controlled electron impact ion source where the electron energy is variable from 1 to 100 eV. Ionizing electrons are emitted from a directly heated tungsten carbide filament, collimated into a beam, and accelerated into the source region where ionization occurs. The energy of ionizing electrons in the ion source has been calibrated by comparing measured and known values of the ionization potentials for rare gas atoms and for diatomic molecules. A slight ion-repeller voltage is applied to backing plates in the source in order to repel ions into the slit system for acceleration to terminal velocities. Figure 1 presents a schematic diagram of the experimental apparatus in which the relative distances are drawn to scale. A

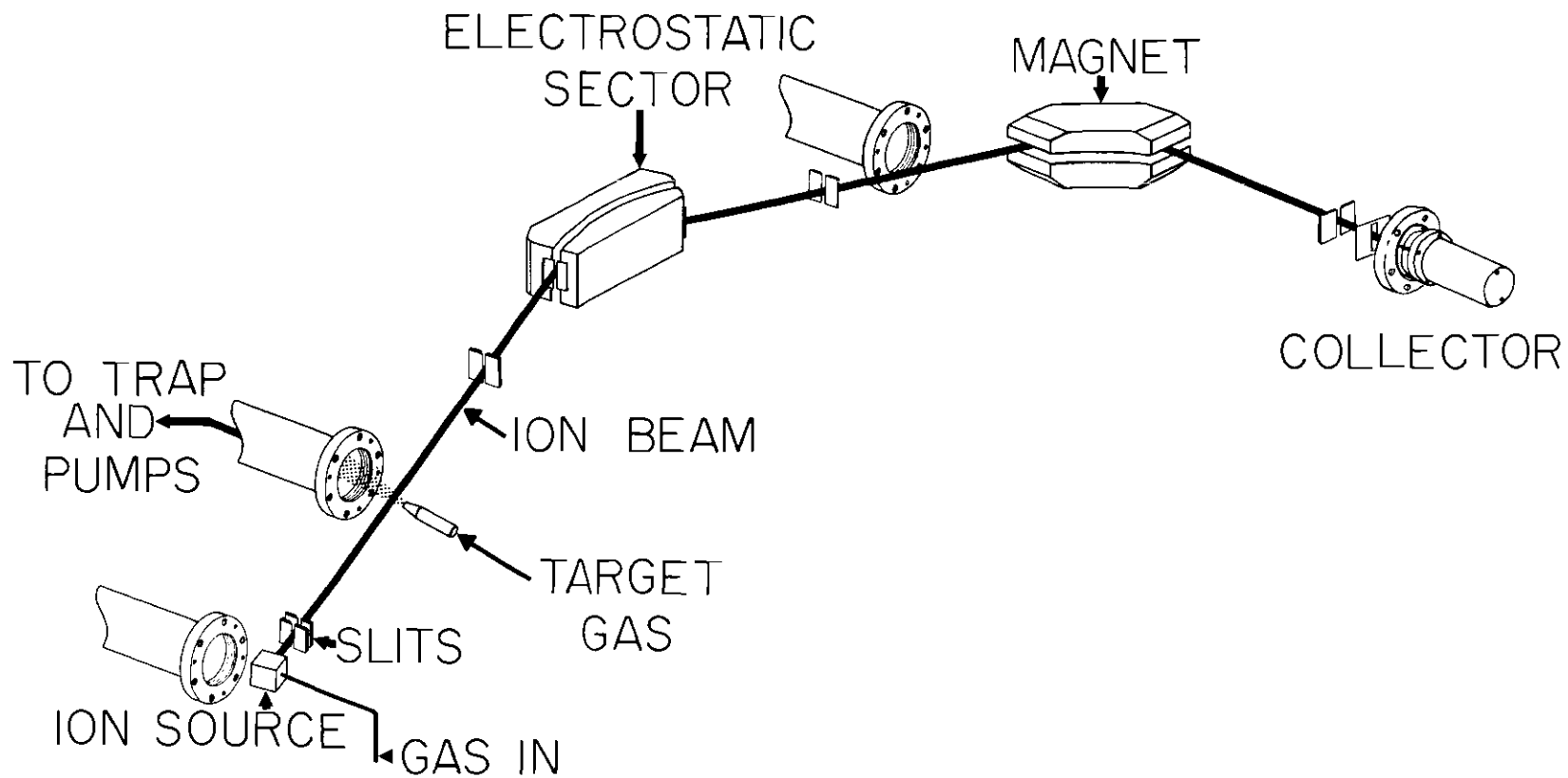


Figure 1. Schematic Diagram of Apparatus Used to Study Ionization Efficiency Curves.

focused, fully accelerated ion beam emerges from the ion source-acceleration slit region and enters the main drift tube. The main drift tube possesses variable collimating slits and a separate pumping system.

Ions emerging from the source region collide with a beam of neutral molecules issuing from a jet. The neutral beam is aimed at a  $90^\circ$  angle with respect to the ion beam. After crossing the ion beam, the neutral beam passes directly into the pumping system. Directing the neutral beam into the pumping system maintains a low background pressure in the drift space and minimizes ion-molecule interactions outside the collision region defined by the intersection of the ion and the neutral beams.

Having passed through the collision region ions next enter a  $45^\circ$  electrostatic sector for energy analysis. Energy selected ions exiting this sector are then momentum analyzed with a  $90^\circ$  magnet with a 20 cm radius.

#### Product Identification

The condition for a particle of charge  $Ze$ , mass  $m$  and velocity  $v$  to describe a circular path through the electrostatic sector is one in which the force of the field must equal the centrifugal force on the particle. This condition is given by

$$mv^2/r_0 = - A/r_0 \quad (7)$$

where  $r_0$  is the mean radius of the sector and  $A$  is a constant of the field. In terms of voltages,  $V'$ , on the sector

$$\Delta V'_{\text{sector}} = V'_{r_2} - V'_{r_1} = \frac{w_{r_2 - r_1}}{Ze} = \frac{1}{Ze} \int_{r_1}^{r_2} F dr = \frac{1}{Ze} \int_{r_1}^{r_2} \left(-\frac{A}{r}\right) dr \quad (8)$$

where  $w_{r_2 - r_1}$  is the work required to move a charge  $Ze$  from the inner plate  $r_1$  to the outer plate  $r_2$ . This equation gives

$$\Delta V'_{\text{sector}} = \frac{1}{Ze} (-A) \ln r_2/r_1 \quad (9)$$

$$A = -Ze \Delta V' / \ln(r_2/r_1) . \quad (10)$$

Substituting in the above equation

$$mv^2/r_0 = -A/r_0 = Ze\Delta V' / r_0 \ln(r_2/r_1) \quad (11)$$

$$mv^2/2 = Ze \Delta V' / 2 \ln(r_2/r_1) = E \quad (12)$$

where  $mv^2/2$  is the kinetic energy  $E$  of the particle.

Ions of charge  $Ze$  produced by electron impact ionization in the ion source are accelerated to terminal velocities by the ion accelerating voltage  $V$ . The kinetic energy of these ions is given by

$$mv^2/2 = ZeV \quad (13)$$

The electrostatic sector will transmit ions when the following condition is met:

$$mv^2/2 = ZeV = Ze\Delta V'/2 \ln(r_2/r_1) \quad (14)$$

$$V = \Delta V'/2 \ln(r_2/r_1) . \quad (15)$$

For our instrument this relation holds for the case that  $\Delta V' = 0.1000V$  since  $2 \ln r_2/r_1$  is 0.1000. Thus, both singly and doubly charged ions of the same  $m$ , which are produced by electron impact in the source experience the full accelerating voltage and are transmitted by the electrostatic sector.

The kinetic energy of the ions emerging from the sector will be given by

$$mv^2/2 = ZeV . \quad (16)$$

These ions next enter the magnetic field for analysis and will reach the collector when the equality

$$BZe v/r = mv^2/r^2 \quad (17)$$

holds. Solving for  $v$  from Equation (17) and substituting it into Equation (16) gives

$$m(B^2 Z^2 e^2 r^2 / m^2) / 2 = ZeV \quad (18)$$

$$m/Ze = B^2 r^2 / 2V . \quad (19)$$

Doubly charged  $N_2^{++}$  ions appear at a mass to charge ratio of 14.003; the same mass to charge ratio as  $N^+$  ions. It is possible for single electron transfer involving  $N_2^{++}$  to occur with the formation of  $N_2^+$  in the collision region between the final ion source accelerating plate and the electrostatic sector. Large impact parameter collisions with little momentum transfer will result in  $N_2^+$  product ions having approximately the same velocity as the incident  $N_2^{++}$  ions. Since the charge on the  $N_2^{2+}$  reactants is  $2e$  and that on the  $N_2^+$  products is  $1e$ , Equation (14) becomes

$$(2)eV = (1)e \Delta V' / 2 \ln(r_2/r_1) \quad (20)$$

and

$$\Delta V' = 2(V_2 \ln(r_2/r_1)) \quad (21)$$

which is twice the sector voltage necessary to pass the reactant  $N_2^{++}$  ions. The product  $N_2^+$  ions passing through the sector next enter the magnetic field and are focussed at mass 56.012 since

$$mv^2/2 = (Z)eV \quad (16)$$

and

$$(Z/(z-1)^2)(m/e) = 2(m/e) = B^2 r^2 / 2V \quad (22)$$

when  $Z$  is 2. The combination of double the normal sector voltage

required to pass the product ions and location of the mass at 56 positively identifies the  $N_2^+$  product from the



reaction.

Any  $N^+$  products from the dissociative channels in Reaction (23) will have approximately the same velocity as the reactant  $N_2^{++}$  ions. Rather than being transmitted by a sector voltage of  $2(V/2 \ln(r_2/r_1))$ , these  $N^+$  products are transmitted by half this voltage since

$$m_{N_2^{2+}} v_{N_2^{2+}}^2 / 2 = (2)eV \quad (24)$$

and

$$(1/2)(m_{N_2^{2+}} v_{N_2^{2+}}^2) / 2 = (2)(eV) / 2 = e\Delta V' / 2 \ln(r_2/r_1) \quad (25)$$

$$(m_{N^+} v_{N^+}^2) / 2 = eV = e\Delta V' / 2 \ln(r_2/r_1) \quad (26)$$

$$V = \Delta V' / 2 \ln(r_2/r_1) \quad (27)$$

which is the normal sector voltage, Equation (15), used to transmit ions produced in the electron beam, accelerated, and passed through the accelerating potential  $V$ .

These  $N^+$  product ions will be analyzed by the magnetic field and focused at a nominal mass of 14.003 if  $v_{N^+} = v_{N_2^{2+}}$ . This is shown by

the following equations:

$$m_{N^+} v_{N_2^{2+}}^2 / 2 = (2)eV / 2 \quad (28)$$

$$B(1)eV v_{N_2^{2+}} / r = m_{N^+} v_{N_2^{2+}}^2 / r^2 \quad (29)$$

$$B^2 r^2 / 2V = m_{N^+} / e \quad (30)$$

In these electron transfer processes there is relatively little momentum change of the incident ion due to interaction with the neutral target. Collisions which take place after acceleration but prior to mass analysis give rise to products that appear as a so-called Aston band. The products appear at the mass position

$$(m/Z_e) = [m_f / (Ze)_f]^2 / [m_i / (Ze)_i] \quad (31)$$

where  $m_f / (Ze)_f$  is equal to the mass to charge ratio of the final product and  $m_i / (Ze)_i$  is equal to the mass to charge ratio of the incident ion.

For the following reaction



Equation (31) gives

$$m / (Ze) = (28/1)^2 / (28/2) = 56 .$$

Similarly, for the reaction



Equation (31) yields)

$$m/(Ze) = (14/1)^2/(28/2) = 14$$

The mass 56 and mass 14 peaks obtained by the use of Equation (31) are in agreement with that given in the previous discussion of this Chapter.

#### Time-of-Flight Mass Spectrometer

Obtaining total charge transfer cross sections using a series of target gases with a magnetic mass spectrometer has proven to be difficult. Such measurements using time-of-flight techniques are much simpler and, in addition, the relatively wide collection angle of the time-of-flight apparatus insures all the products of reaction are collected. Total cross sections can be routinely measured using the time-of-flight instrument.

#### Experimental

A brief outline of the time-of-flight mass spectrometer will be given here. Reactant  $\text{N}_2^{++}$  ions have been produced in a controlled electron impact ion source, drawn out of the source region by a fast rising negative pulse, and then accelerated to terminal velocities. The ionizing electrons have been emitted from a directly heated thoria oxide coated filament and accelerated into the ion source region by a

voltage that is continuously variable from 2 to 100 V. A series of collimating holes and an external magnetic field have been used to spatially confine the electron beam and the corresponding point of ion formation. The absolute energy of the electron beam has been checked by measuring ionization potentials of rare gas atoms and diatomic molecules. The electron energy has been monitored during each experiment by a measurement of the  $N_2$  ionization potential. Fine control needle valves, which have been used to admit high purity gases into the respective ion source and collision regions, have provided constant gas densities in different parts of the apparatus. Reactant  $N_2^{++}$  ions produced in the electron impact ionization of  $N_2$  are accelerated to terminal velocities and allowed to interact with neutral molecules in a collision region where charge transfer reactions occur. Neutral  $N_2^+$  products resulting from charge transfer reactions have approximately the same velocity as the incident  $N_2^{++}$  ions. The reactant  $N_2^{++}$  ions have been separated from the fast neutral  $N_2^+$  products by the application of a deceleration voltage placed on a grid assembly, directly in front of the collector, which gives  $N_2^{++}$  ions a slightly longer arrival time than the  $N_2^+$  reaction product. Target gas pressures in the ion-molecule collision region were sufficiently low to ensure that  $N_2^+$  products originate from single bimolecular collisions.

#### Product Identification

Charge transfer reactions involving nitrogen colliding with a target gas produce a variety of products ( $N_2^+$  product,  $N^0$  and  $N^+$ ). These products, along with primary  $N^+$  ions and primary  $N_2^{++}$  ions, will

produce peaks corresponding to their respective flight times in the time-of-flight apparatus. Calculation of the time required for the ion to proceed down the flight tube enables one to identify the peak representing each ion.

The flight tube of the apparatus described above is divided into two parts. Primary ions initially enter a collision region 82.86 cm in length which has a potential of 3 kV. Products of charge transfer reactions and residual primary ions then enter a retarding chamber 13.46 cm in length which has a 1.8 kV potential.

From this information flight times for ions travelling through the tube can be calculated:

$\underline{N_2^{++}}$ : Once inside the 3 kV collision chamber the kinetic energy of the doubly charged ion may be written as:

$$KE_1 = \frac{1}{2}mv_1^2 = 2(3 \text{ kV})(1.6021 \times 10^{-12} \text{ erg/eV})(6.02252 \text{ molecules/mole}) \quad (34)$$

This expression yields a velocity for the ion equal to

$$v_1 = 2.034 \times 10^7 \text{ cm/sec} \quad (35)$$

In a tube of length 82.86 cm an ion with the above velocity will have a flight time,  $t_1$ , given by

$$t_1 = \text{length of tube/velocity} = 4.07 \text{ } \mu\text{sec} \quad (36)$$

Upon entering the retarding chamber (13.46 cm in length) the ion will

experience a potential of 1.8 kV and will possess a kinetic energy

$$KE_2 = \frac{1}{2}mv_2^2 = 2(1.8 \text{ kV})(1.6021 \times 10^{-12})(6.02252 \times 10^{23}) \quad (37)$$

from which  $v_2$  can be calculated.

$$v_2 = 1.575 \times 10^7 \text{ cm/sec} \quad (38)$$

Moving at this velocity,  $v_2$ , the amount of time,  $t_2$ , required to pass through the retarding chamber will be

$$\begin{aligned} t_2 &= 13.46 \text{ cm} / (1.575 \times 10^7 \text{ cm/sec}) \quad (39) \\ &= .85 \text{ } \mu\text{sec} \quad . \end{aligned}$$

Thus, the total flight time for the  $N_2^{++}$  ion is

$$t = t_1 + t_2 = 4.92 \text{ } \mu\text{sec} \quad (40)$$

$N_2^+$ : Derivations of flight times for  $N_2^{++}$  and for  $N^+$  are completely analogous. Although the  $N_2^{++}$  ions has twice the mass of the  $N^+$  ion, it also has twice the kinetic energy of the  $N^+$  ion by virtue of its double charge. Therefore, the flight time for the  $N^+$  ion will also be 4.92  $\mu\text{sec}$ .

$N_2^+$  Product: After entering the collision region  $N_2^{++}$  may pick up an electron to form  $N_2^+$  prod. Note that although the charge of the

$N_2^{++}$  species is reduced by one in forming  $N_2^+$  prod, the kinetic energy of the  $N_2^+$  prod must still equal that of the  $N_2^{++}$  for large impact parameter collisions.

$$KE_1 = \frac{1}{2}mv_1^2 =$$

$$2(3.0 \text{ kV})(1.6021 \times 10^{-12} \text{ erg/eV})(6.02252 \times 10^{23} \text{ molecule/mole}) \quad (41)$$

$$v_1 = 2.034 \times 10^7 \text{ cm/sec} \quad (42)$$

$$t_1 = 82.86 \text{ cm}/v_1 = 4.07 \text{ } \mu\text{sec} \quad (43)$$

Proceeding from the collision chamber to the retarding chamber, one finds a drop in voltage from 3 kV to 1.8 kV. This drop is equivalent to a retarding potential of 1.2 kV. The potential experienced by the  $N_2^+$  prod ion in the retarding chamber will equal the potential it experienced in the collision chamber minus the retarding potential. Using this expression for total potential the kinetic energy can be written as:

$$KE_2 = \frac{1}{2}mv_2^2 = [2E_1 - 1.2 \text{ kV}](1.6021 \times 10^{-12})(6.02252 \times 10^{23}) \quad (44)$$

After solving for  $v_2$  the flight time,  $t_2$ , for the passage of the ion through the retarding chamber is found.

$$v_2 = 1.819 \times 10^7 \text{ cm/sec} \quad (45)$$

$$t_2 = 13.46 \text{ cm}/v_2 = .74 \text{ } \mu\text{sec} \quad (46)$$

The total flight time will be

$$t = t_1 + t_2 = 4.81 \text{ } \mu\text{sec} \quad (47)$$

N<sup>0</sup>: Uncharged nitrogen, N<sup>0</sup>, is formed from N<sup>+</sup> via the acquisition of an electron. An uncharged species will experience no retarding potential, allowing the atom to move through the tube at a constant velocity. Writing the kinetic energy expression yields a velocity for N<sup>0</sup> equal to:

$$KE = \frac{1}{2}mv^2 = (3 \text{ kV})(1.6021 \times 10^{-12})(6.02252 \times 10^{23}) \quad (48)$$

$$v = 2.034 \times 10^7 \text{ cm/sec} \quad (49)$$

A flight time,  $t$ , can then be calculated for N<sup>0</sup>:

$$t = (13.46 \text{ cm} + 82.86 \text{ cm})/2.034 \times 10^7 \text{ cm/sec} \quad (50)$$

$$= 4.74 \text{ } \mu\text{sec} \quad .$$

N<sup>+</sup><sub>product</sub>: Dissociation of N<sub>2</sub><sup>++</sup> within the collision region may produce two N<sup>+</sup><sub>prod</sub> ions each with  $\frac{1}{2}$  the kinetic energy of the N<sub>2</sub><sup>++</sup> ion. Since the flight time of N<sup>+</sup><sub>prod</sub> in the collision region is identical to the flight time for an N<sub>2</sub><sup>++</sup> ion through the collision region,

$t_1 = 4.07 \mu\text{sec}$ . However, after dissociation the kinetic energy of each  $N_{\text{prod}}^+$  fragment is only  $\frac{1}{2}$  that of the  $N_2^{++}$  ion. For this reason, flight times for  $N_{\text{prod}}^+$  through the retarding chamber and for  $N_2^{++}$  through the retarding chamber will differ. One can calculate  $t$  for  $N_{\text{prod}}^+$  as shown below.

$$KE_2 = \frac{1}{2}mv_2^2 = [3.0 \text{ kV} - 1.2 \text{ kV}](1.6021 \times 10^{-12})(6.02252 \times 10^{23}) \quad (51)$$

$$v_2 = 1.575 \times 10^7 \text{ cm/sec} \quad (52)$$

$$t_2 = .85 \mu\text{sec} \quad (53)$$

$$t = t_1 + t_2 = 4.92 \mu\text{sec} \quad (53)$$

The discussion above indicates the presence of three peaks appearing in the order of their respective flight times (ions with shortest flight times will appear first). Note that the flight times for the three ions  $N_2^{++}$ ,  $N^+$  and  $N_{\text{prod}}^+$  are all equal to  $4.92 \mu\text{sec}$ . The peak corresponding to a flight time of the  $N_2^{++}$  is sufficiently different to be clearly separated from these other three ions.

## CHAPTER III

## POTENTIAL ENERGY CURVES

Scientific studies involving the ionization potentials of doubly charged molecules have necessitated theoretical estimates of these quantities. The use of conventional quantum mechanical methods would be expected to encounter difficulties when applied to energy calculations of doubly charged systems. Even with the removal of two electrons from  $N_2$ , there are a sufficient number of electrons remaining in  $N_2^{++}$  to render ab initio calculations long and tedious. However, A.C. Hurley has developed an alternate approach, to obtaining appearance potential, based upon the quantum mechanical virial theorem.<sup>4</sup> Hurley's approach, presented below, utilizes an approximate relationship between the potential curves of the doubly charged ion and the potential curve of a related neutral molecule.

Define  $E(s)$ ,  $T(s)$  and  $V(s)$  to be the total energy, mean kinetic energy, and mean potential energy of a polyatomic molecule,  $A_1, A_2, \dots, A_N$ , with nuclei at the points  $sR_1, sR_2, \dots, sR_N$ . When  $s$  becomes large ( $R_N$  remaining fixed) the molecule in the ground state  $X$  will dissociate into  $A_1^{Q_1}, A_2^{Q_2}, \dots, A_N^{Q_N}$ , where  $Q_i$  is the charge on the fragment  $A_i$ . Thus, the binding energy  $B(R_i)$  for this nuclear configuration is given by

$$B(R_i) = E(\infty) - E(1) = - \sum_{i < j}^N (Q_i Q_j / R_{ij}) + \int_1^{\infty} \{T(\infty) - T(s)\} ds, \quad (55)$$

where  $R_{ij} = |R_i - R_j|$ .

It is advantageous, when dealing with diatomic systems, to express  $T$  as a function of  $sR$  rather than as a function of  $s$ , the scale factor.

$$B(R) = - [(Q_1 Q_2) / R] + \int_1^{\infty} \{T(\infty) - T(sR)\} dsR \quad (56)$$

$$= - [(Q_1 Q_2) / R] + (1/R) \int_R^{\infty} \{T(\infty) - T(R')\} dR' \quad (57)$$

The variable  $R$  in the above equations represents the nuclear separation. Since the second ionization potential of an atom is much greater than the first, the ground state and low lying excited states of a doubly charged diatomic ion ( $d$ ) will usually dissociate adiabatically into two singly charged ions. For this case,  $Q_1 = Q_2 = 1$  and Equation (57) may be written:

$$B_d(R) = (1/R) + (1/R) \int_R^{\infty} \{T_d(\infty) - T_d(R')\} dR' \quad (58)$$

In going from the neutral molecule to the doubly charged species an approximately uniform contraction in the wavefunction will occur due to the larger nuclear charge. For homonuclear or for almost homonuclear ions  $T_d$  can be evaluated using the wavefunction:

$$\psi_d(t, R; x_i) = t^{3m/2} \psi_n(tR_i; tx_i) \quad (59)$$

where  $t$  is a variable scaling factor and  $t^{3m/2}$ ,  $m$  being equal to the number of electrons, ensures that  $\psi_d$  is normalized.

From Equation (59)

$$T_d(R) = t^2 T_n(tR) , \quad (60)$$

and using this relationship in Equation (58),

$$B_d(R) = - (1/R) + (1/R) \int_R^\infty \{t^2(\infty) T_n(\infty) - t^2(R') T_n(tR')\} dR' . \quad (61)$$

Using an approximation of the constant  $t$ , determined at infinite nuclear separation, Equation (62) can be derived from Equation (60):

$$t(R) = t(\infty) = \{[T_d(\infty)]/[T_n(\infty)]\}^{1/2} . \quad (62)$$

In addition, from Equation (61),

$$B_d(R) = - (1/R) + [t^2(\infty)/R] \int_R^\infty \{T_n(\infty) - T_n[t(\infty)R']\} dR' . \quad (63)$$

Using Equation (57) and assuming that the neutral molecule dissociates adiabatically into neutral atoms,

$$B_n[t(\infty)R] = [1/t(\infty)R] \int_{t(\infty)R}^\infty \{T_n(\infty) - T_n(R')\} dR' \quad (64)$$

$$= (1/R) \int_R^\infty \{T_n(\infty) - T_n[t(\infty)U]\} dU , \quad (65)$$

so that,

$$B_d(R) = - (1/R) + t^2(\infty) B_n\{t(\infty)R\} . \quad (66)$$

Consequently,  $B_d(R)$  can be calculated by using Equation (62), Equation (66), the potential energy curve for the corresponding state of the isoelectronic neutral molecule, and the electronic kinetic energy of the dissociation products. The derivation of Equation (66) contains two basic approximations. Initially, Equation (59) assumes that the wavefunction  $\psi_d$  may be obtained by rescaling  $\psi_n$ . This leads to accurate results only when  $t(\infty)$  lies within the interval  $1 \leq t(\infty) \leq 1.5$  (this range includes most cases of physical interest and includes all cases dealt with in this manuscript). Secondly, Equation (62) assumes that the optimum scale factor is independent of  $R$ ; however, studies show that Equation (62) always supplies a good approximation to the optimum  $t(R)$ .

A somewhat better calculation of  $B_d(R)$  is to modify Equation (62) and Equation (66) by considering electrons in the valence shell apart from those in inner shells. If Equation (62) and Equation (66) are reevaluated according to the above modification, one obtains equations similar in form to those given previously, which are

$$t(R) = t(\infty) = \{T_{d,v}(\infty)/T_{n,v}(\infty)\}^{1/2} \quad (67)$$

$$B_d(R) = - (1/R) + t^2(\infty) B_n\{t(\infty)R\} . \quad (68)$$

Potential energy curves for the systems under consideration in this paper are presented in Figures 2 through 5. Spectroscopic constants, used in subsequent chapters to obtain information on the vibrational overlaps, that are tabulated in Table 1 have been taken from Hurley's curves.

Table 1. Spectroscopic Constants for States of  $N_2^{++}$ ,  $O_2^{++}$  and  $NO^{++}$ 

	State	$r_e (10^{-8} \text{ cm})$	$\omega_e$	$\omega_e X_e$
$N_2^{++}$	$X^3\Pi_u$	1.222	1505	17.7
	$X^1\Sigma_g^+$	1.148	1724	21.2
	$A^1^3\Sigma_g^-$	1.295	1253	20.3
	$b^1\Pi_u$	1.235	1425	19.0
	$A^3\Pi_g$	1.180	1518	27.2
	$c^1\Pi_g$	1.179	1596	25.2
	$d^1\Sigma_u^+$	1.149	1675	21.3
$O_2^{++}$	$X^1\Sigma_g^+$	1.010	2363	19.4
	$A^3\Sigma_u^+$	1.285	952	38.4
	$B^3\Pi_g$	1.163	1405	23.5
	$B^1^3\Sigma_u^-$	1.246	1170	20.6
	$a^1^1\Sigma_u^-$	1.239	1204	19.8
	$\omega^1\Delta_u$	1.212	1453	13.6
	$a^1\Pi_g$	1.175	1367	22.5
	$C^3\Pi_u$	1.080	1777	26.1
$NO^{++}$	$X^2\Sigma^+$	1.082	2032	18.4
	$A^2\Pi$	1.154	1662	19.0
	$B^2\Sigma^+$	1.067	1908	31.5

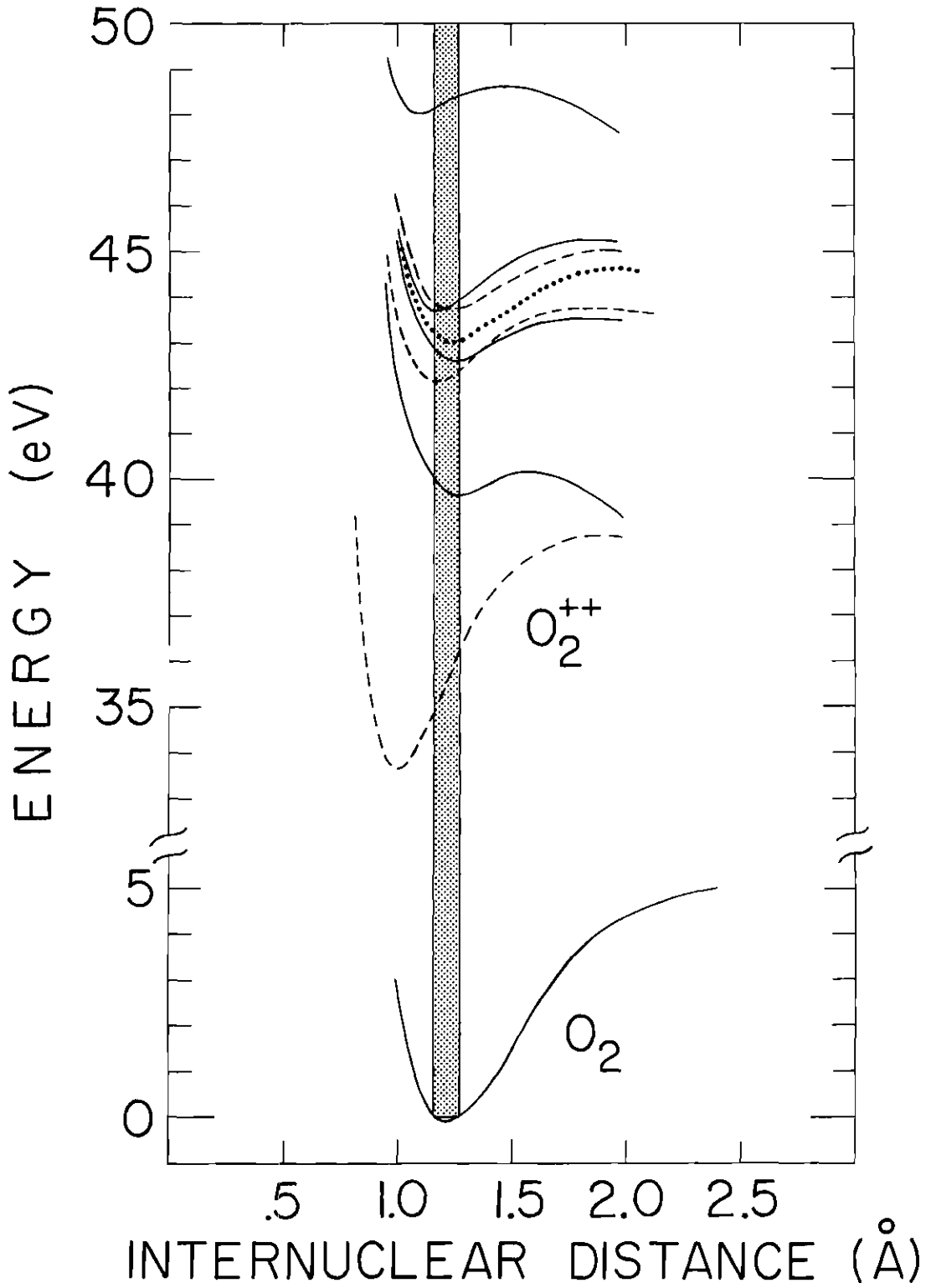


Figure 2. Potential Energy Curves of the Ground State of  $O_2$  and the Excited States of  $O_2^{++}$ , as Predicted by Hurley.<sup>2</sup>

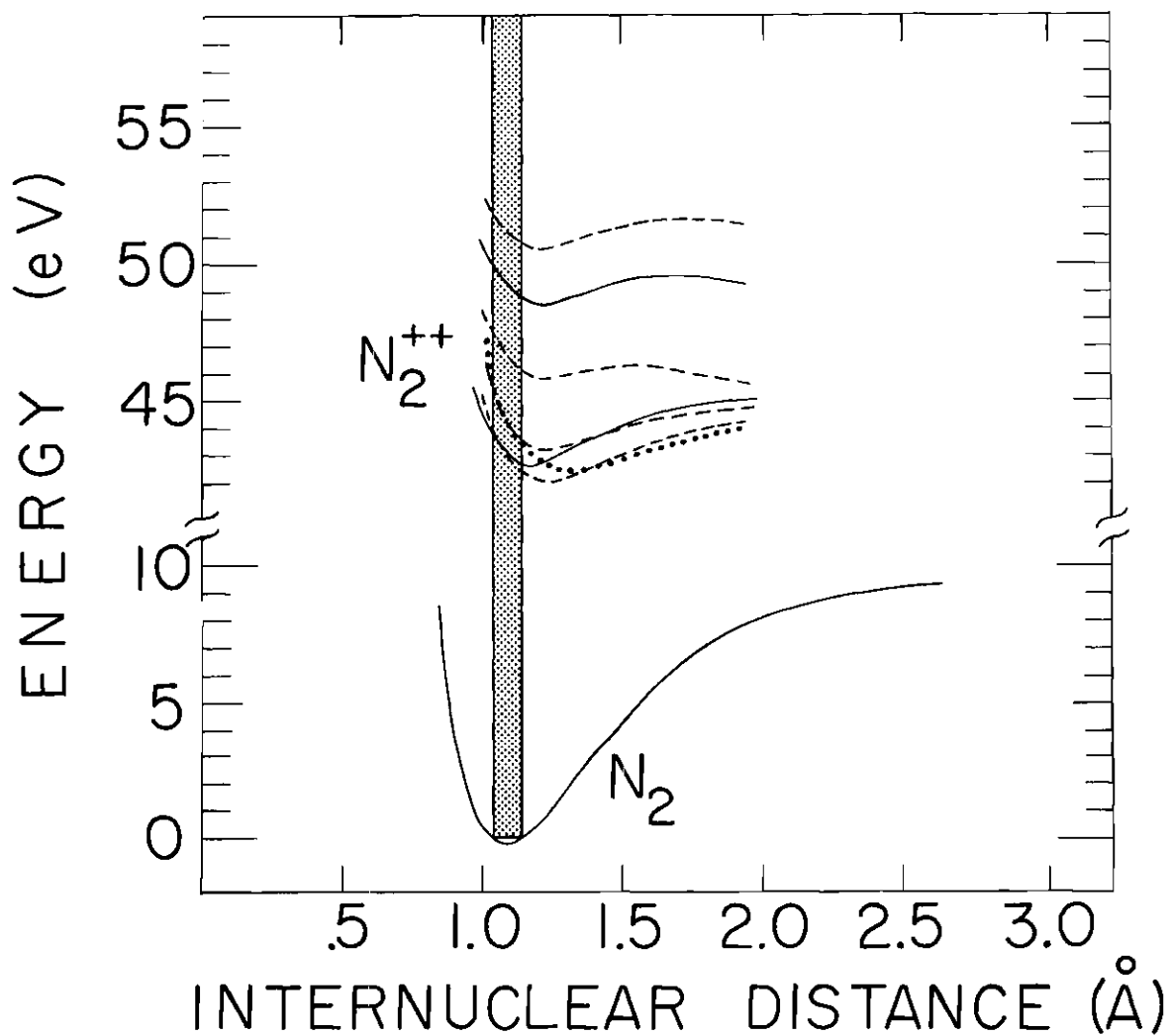


Figure 3. Potential Energy Curves of the Ground State of  $N_2$  and the Excited States of  $N_2^{++}$ , as Predicted by Hurley.

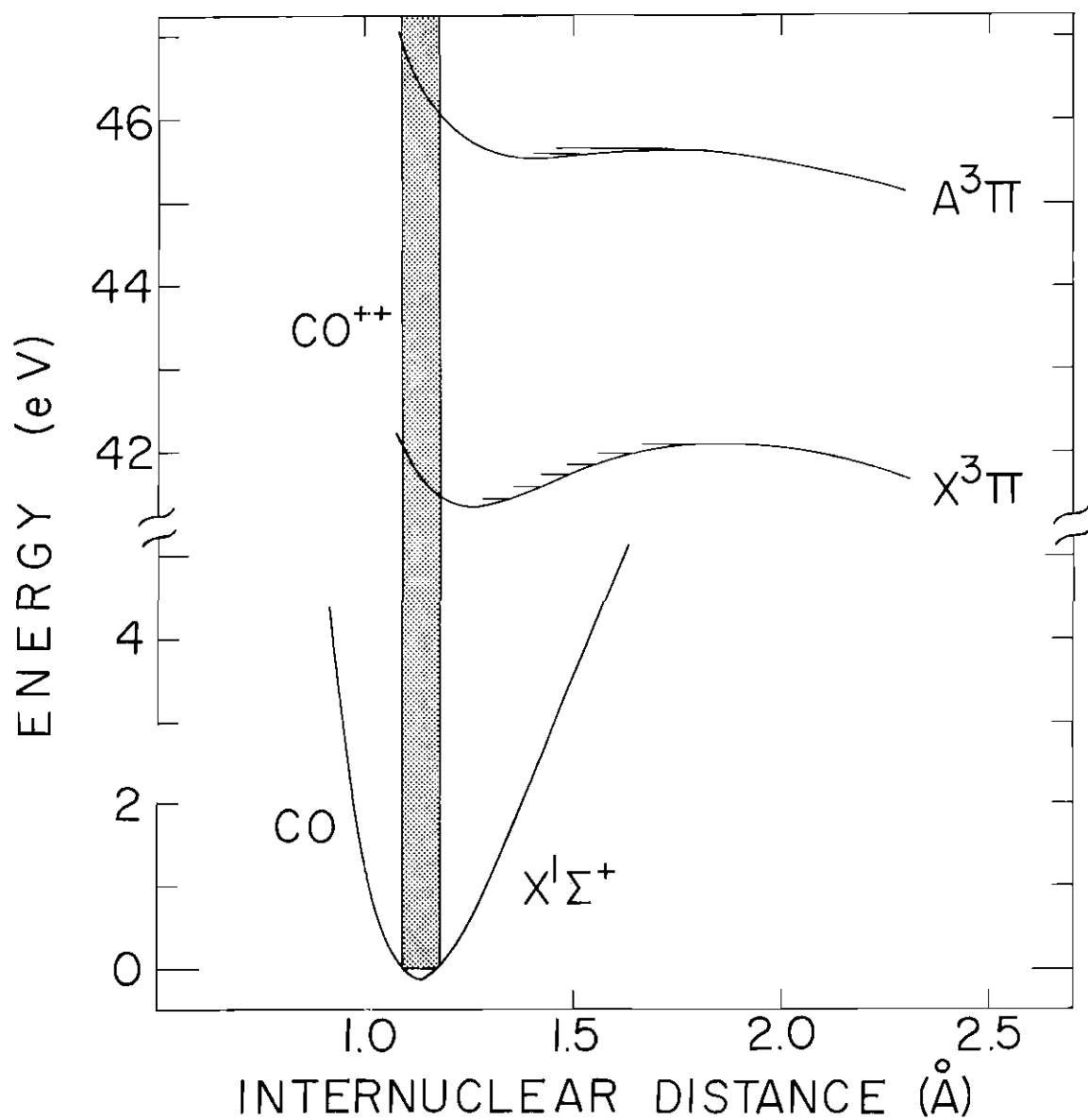


Figure 4. Potential Energy Curves of the Ground State of CO and the Excited States of  $\text{CO}^{++}$ , as Predicted by Hurley.

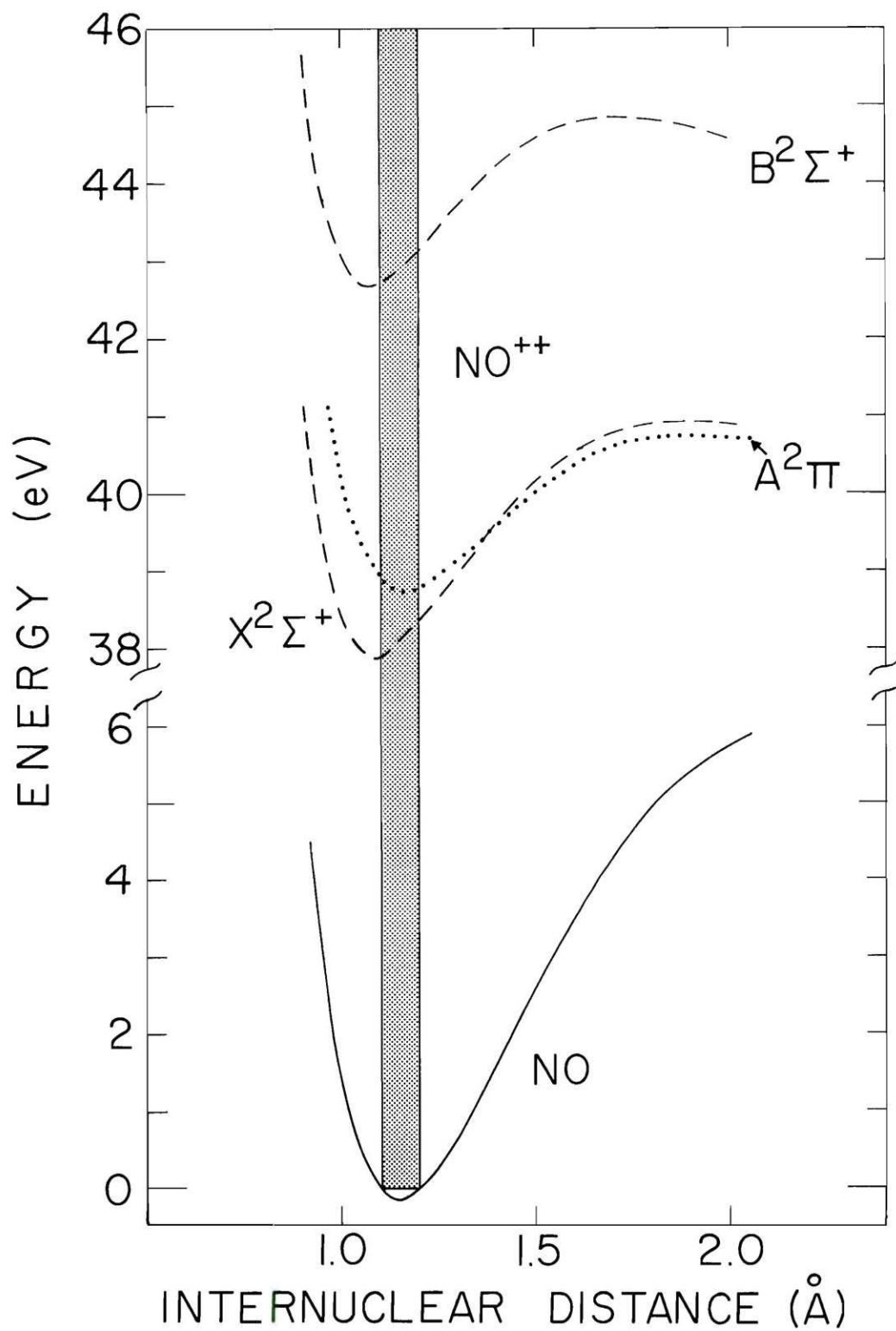


Figure 5. Potential Energy Curves of the Ground State of NO and the Excited States of NO<sup>++</sup>, as Predicted by Hurley.

## CHAPTER IV

### IONIZATION POTENTIALS

#### Introduction

Available methods for finding the ionization potential of an ion depend upon accurate measurement of the ionization efficiency curve for the ion. The ion being considered is normally introduced at a suitable pressure and is then ionized by an electron beam, the energy of which may be varied. Determination of the molecular ionization potential then becomes a task of evaluating the minimum energy required for the formation of the ions.

Due to field penetration within the instrument, the true electron energy may vary considerably from that registered on an external voltmeter. Obviously, such variations must be assessed in order to properly calibrate the electron energy scale. This can be achieved by the introduction of a calibrating gas into the chamber, along with the sample gas. The electron energy scale may then be correctly calibrated by comparing the appearance potential of the calibrating gas to its true ionization potential.<sup>5</sup>

#### Theory

Studies carried out by F.H. Dorman, J.D. Morrison and others<sup>6,7</sup> indicate that processes involving  $n$ -fold, electron impact induced ionization in monoatomic gases have ionization probabilities which vary above threshold as the  $n^{\text{th}}$  power of the excess electron energy.<sup>8</sup>

Double ionization in molecules also abides by a threshold law where the probability of double ionization is a square-law function of excess electron energy. This threshold law for double ionization has received support from the theoretical models of Sydney Geltman<sup>9</sup> and G.H. Wannier.<sup>10</sup>

Geltman has studied the behavior of the cross-section for ionization by electron impact. Investigations were carried out in the vicinity of the threshold by means of the quantum theory of inelastic scattering. Interaction between the incident electrons and the atomic electrons is considered as the perturbation. The electron-nuclear interaction is contained within the unperturbed Hamiltonian for the problem. From this work Geltman shows that the limiting law for hydrogen atom ionization has a linear dependence on the excess incident energy while for double ionization it has a square dependence on the excess incident energy. Statistical-mechanical arguments proposed by Wannier also predict a  $n^{\text{th}}$  power threshold law for  $n$ -fold ionization in agreement with experimentation.

Following arguments based on the Franck-Condon principle, Coolidge, James and Present<sup>11</sup> have shown that the probability of an ionizing transition occurring from vibrational level  $v'' = 0$  of the target molecule in electronic state  $i$ , to vibrational level  $v'$  of the ionic state  $j$  is given by

$$P_{i v', j v''=0} = K(V - V_{v'})^2 [R_{ij} e^2 |\langle \psi_{v'} | \psi_{v''=0} \rangle|^2] . \quad (69)$$

The value of  $K$  in Equation (69) remains constant;  $(V - V_{v'})$  represents

the excess electron energy above the excitation threshold; and the bracketed term is the overlap integral. High energy electron impact occurs for above the excitation threshold so  $(V - V_{v_1})$  is essentially constant.

### Experimental Results

Experimental measurements of ionization potentials, utilizing ionization efficiency curves, are presented in Table 2. These experimental values are very similar to the literature values shown in Table 3.

The ionization efficiency curves for the reaction



is illustrated in Figure 6. Inspection of the ionization efficiency curves for  $\text{Ar}^+(m/e = 80)$  and for  $\text{Ar}^{++}(m/e = 20)$  reveals that their shapes are almost identical. This indicates that all excited states of  $\text{Ar}^{++}$  that are populated have the same reaction cross section. At an electron energy of approximately 56 eV, the ion intensity scale is magnified by a factor of 5. A plot of the square-root of ion intensity versus electron energy produces a linear relationship which can be extrapolated to a threshold value equal to 43.2 eV. Thus, the ionization potential of  $\text{Ar}^{++}$  may be taken to be 43.2 eV, as indicated by the arrow which shows the current literature value.

Ionization efficiency curves for all systems contained in Table 2 are found in Figures 6 through 13. Arrows in the figures indicate

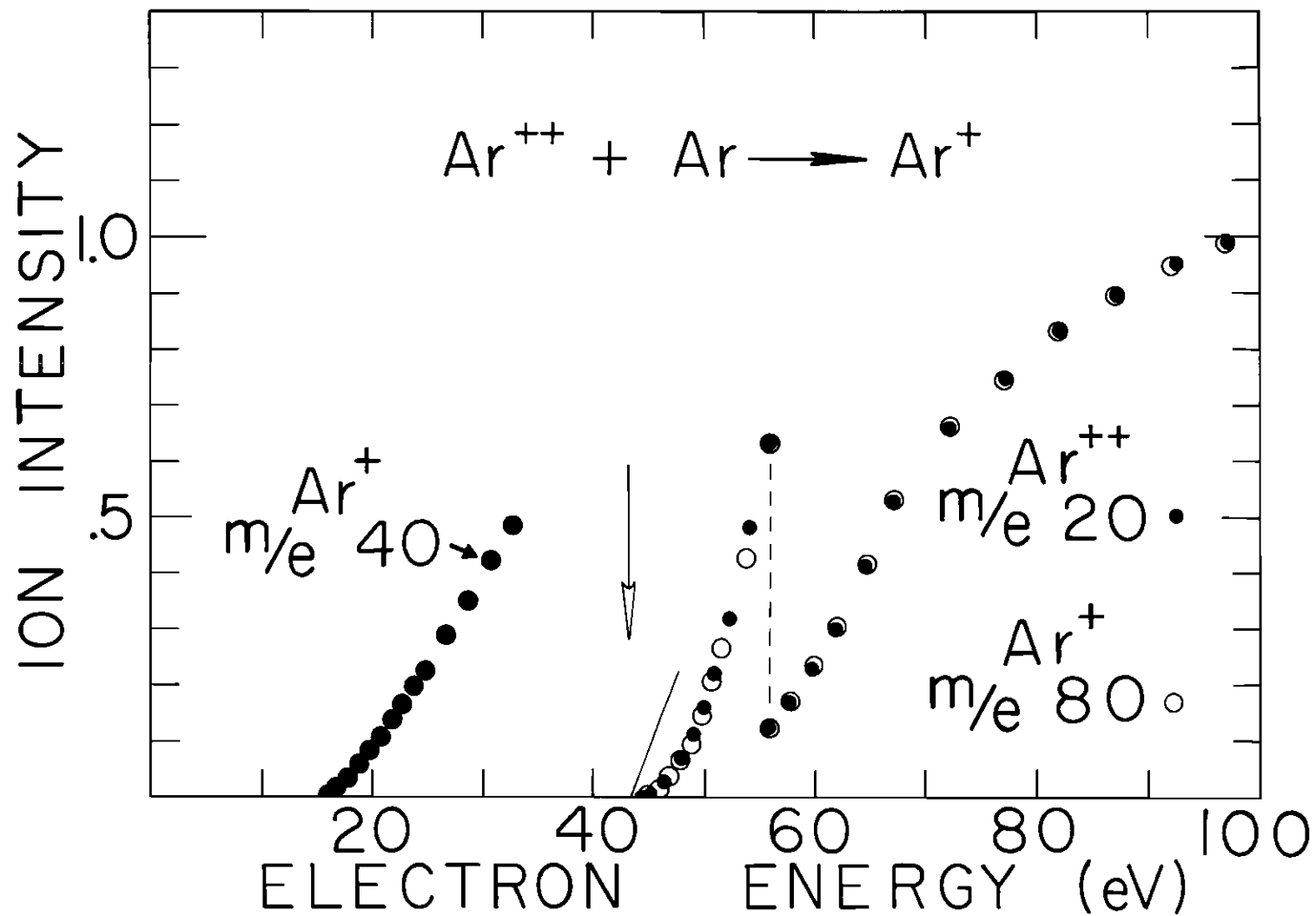


Figure 6. Ionization Efficiency Curves for Species Involved in the Reaction:  $\text{Ar}^{++} + \text{Ar} \rightarrow \text{Ar}^+$ .

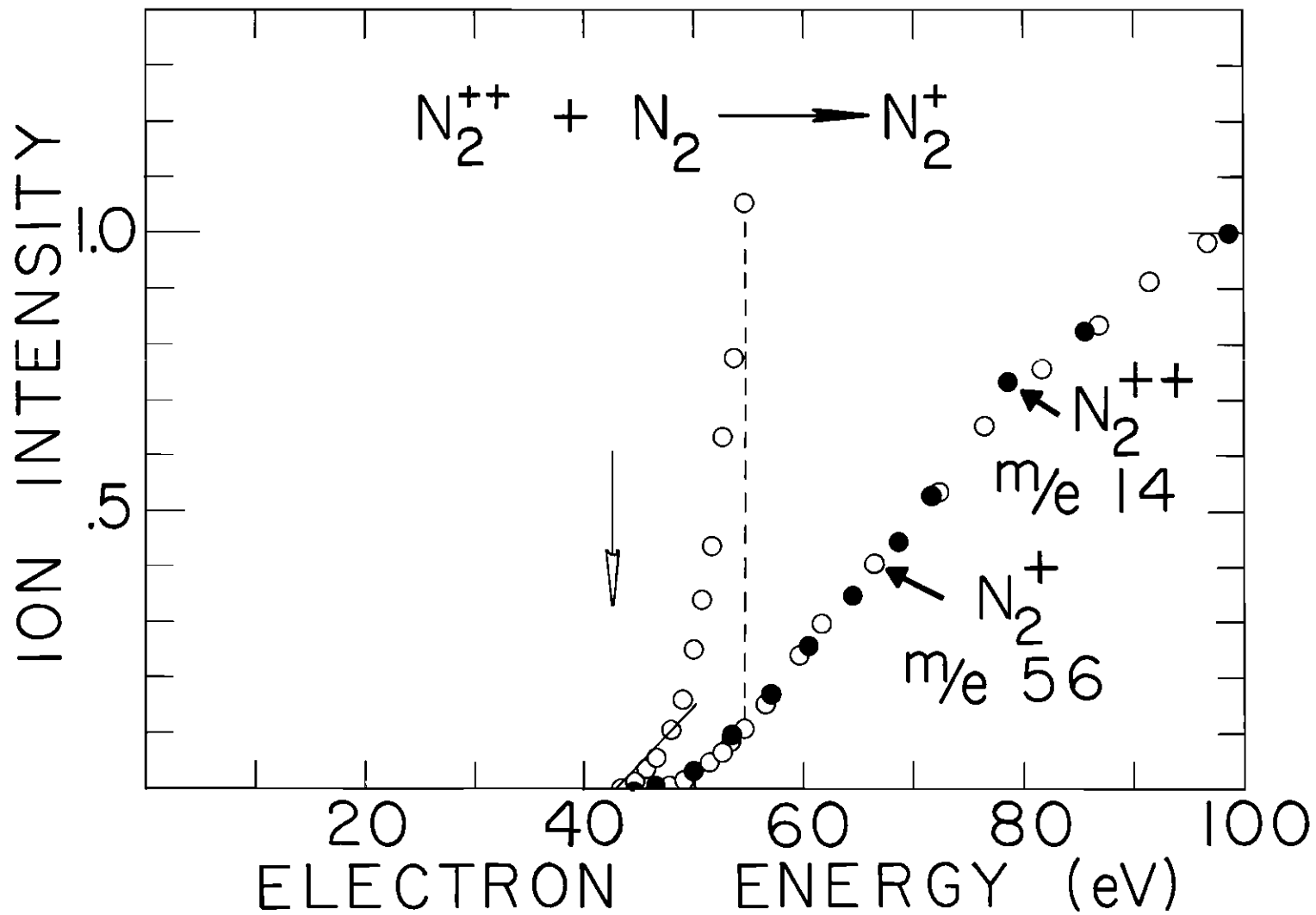


Figure 7. Ionization Efficiency Curves for Species Involved in the Reaction:  $N_2^{++} + N_2 \rightarrow N_2^+$ .

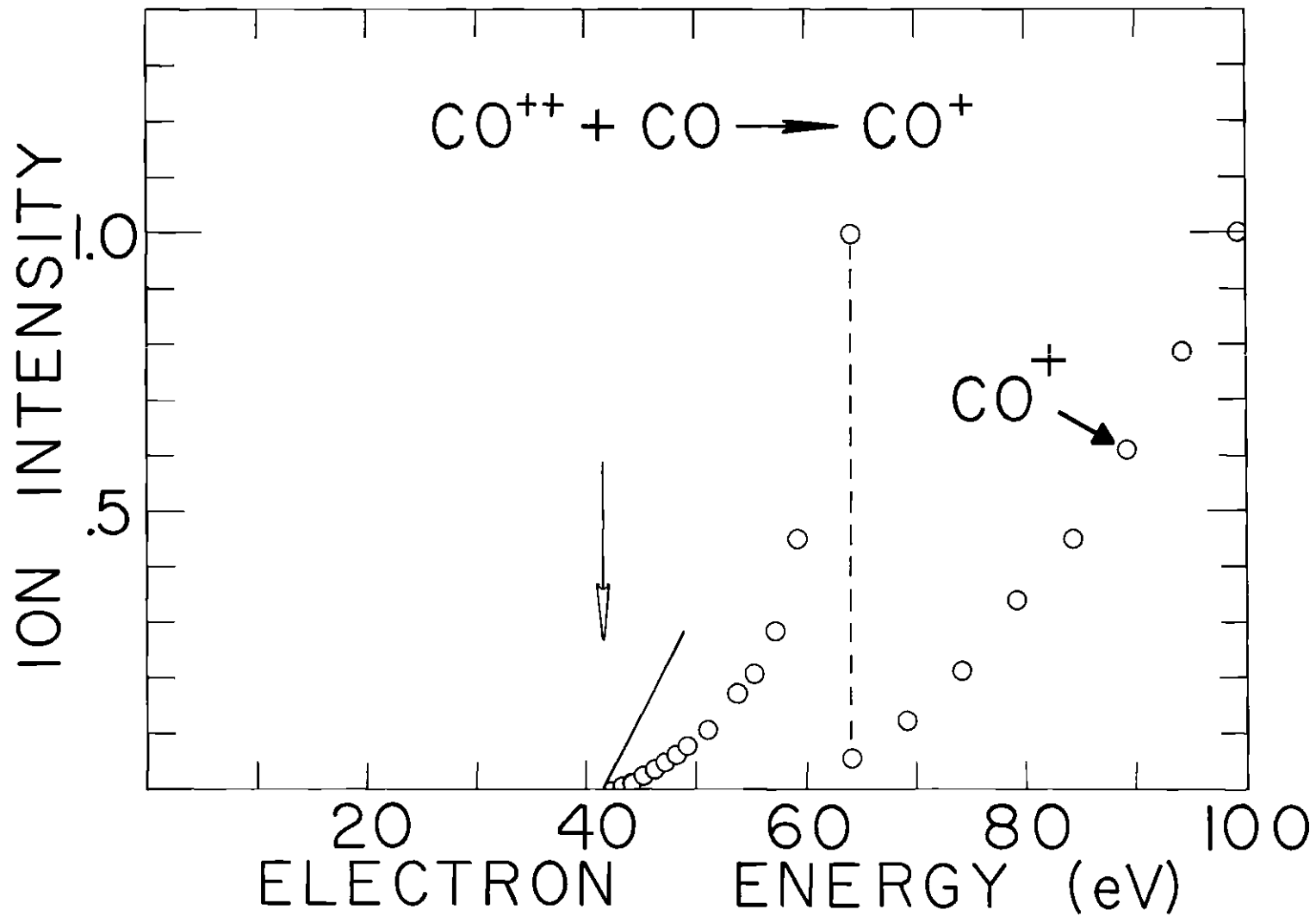


Figure 8. Ionization Efficiency Curve of  $\text{CO}^+$  Involved in the Reaction:  $\text{CO}^{++} + \text{CO} \rightarrow \text{CO}^+$ .

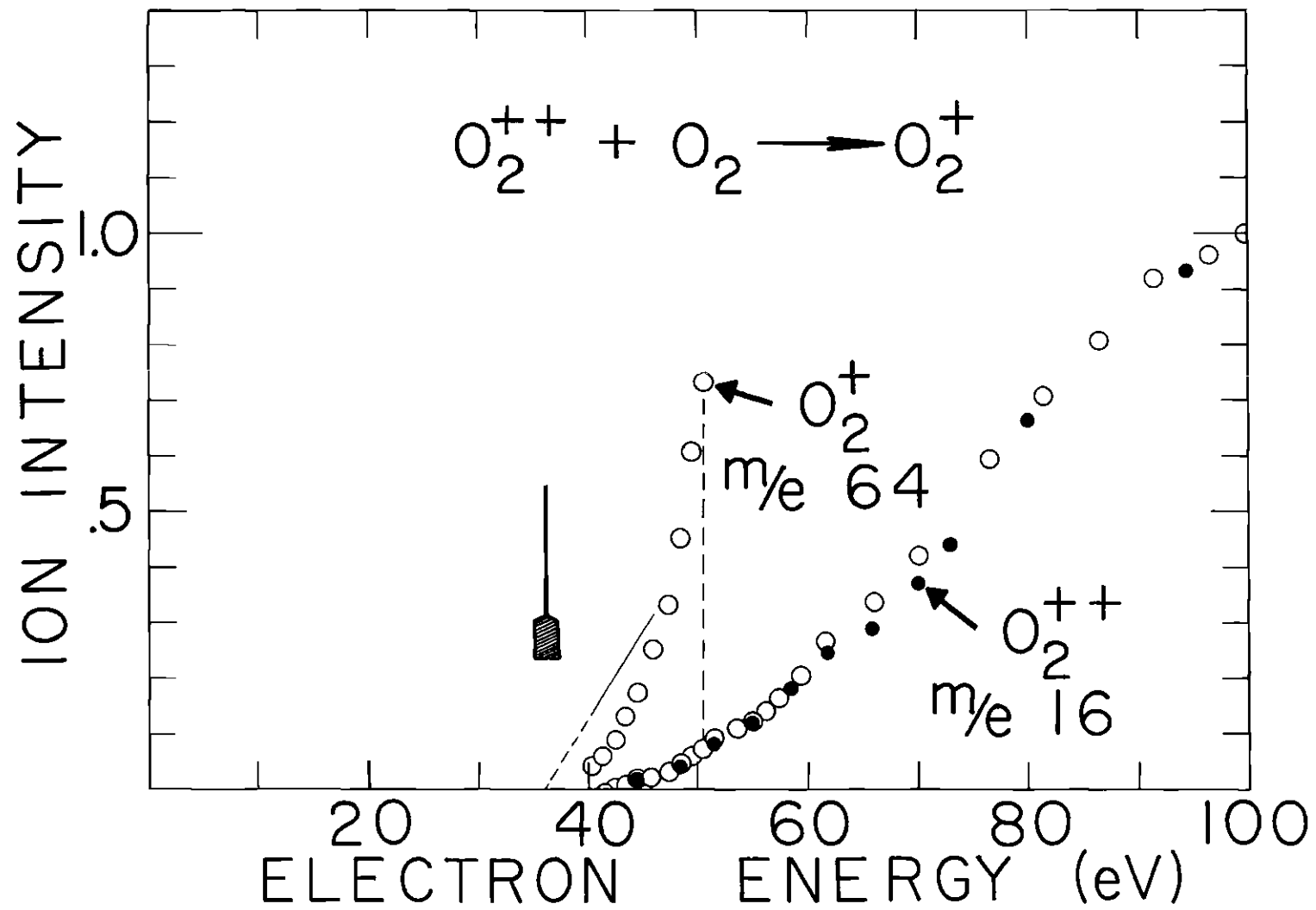


Figure 9. Ionization Efficiency Curves for Species Involved in the Reaction:  $O_2^{++} + O_2 \rightarrow O_2^+$ .

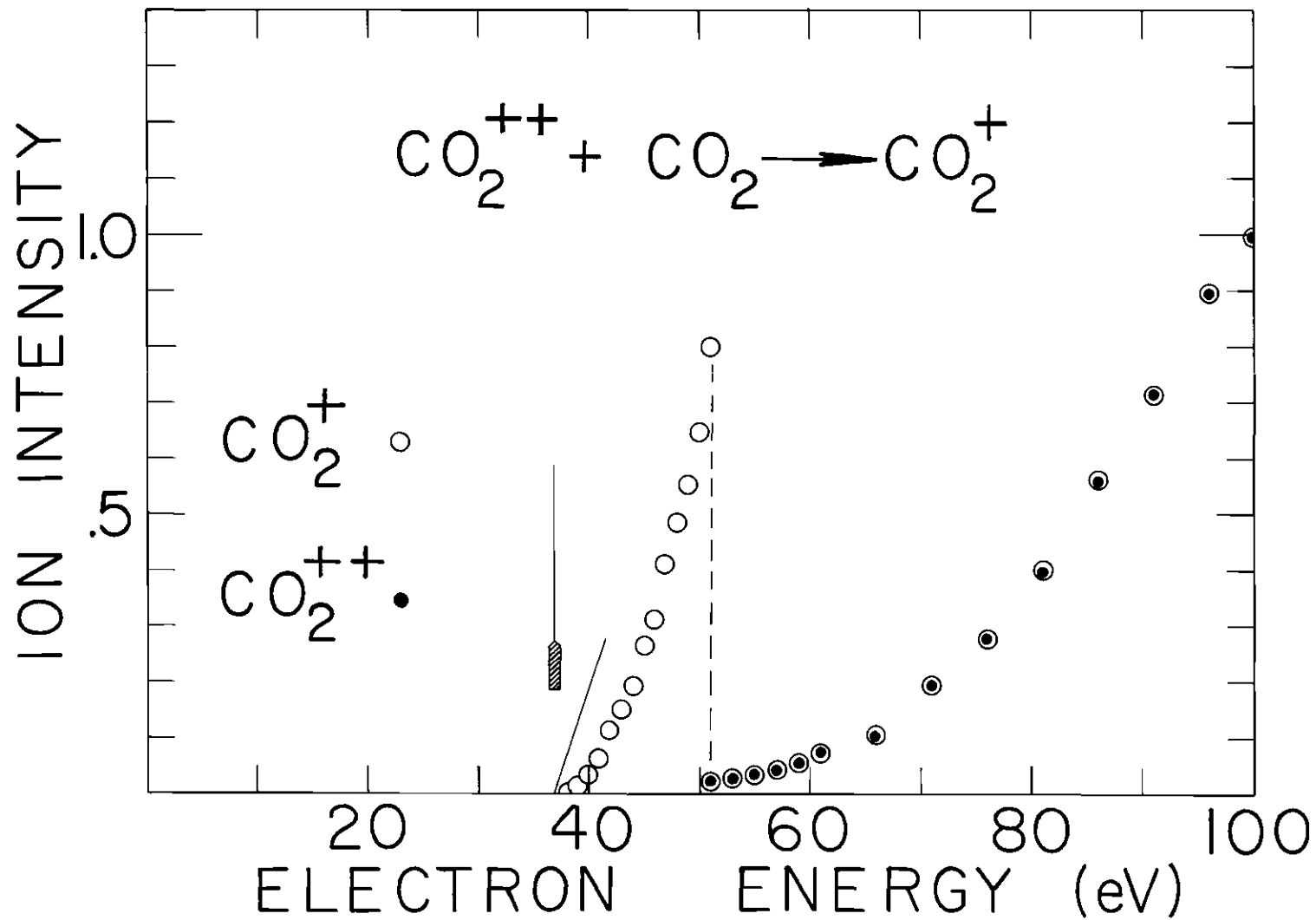


Figure 10. Ionization Efficiency Curves for Species Involved in the Reaction:  $\text{CO}_2^{++} + \text{CO}_2 \rightarrow \text{CO}_2^+$ .

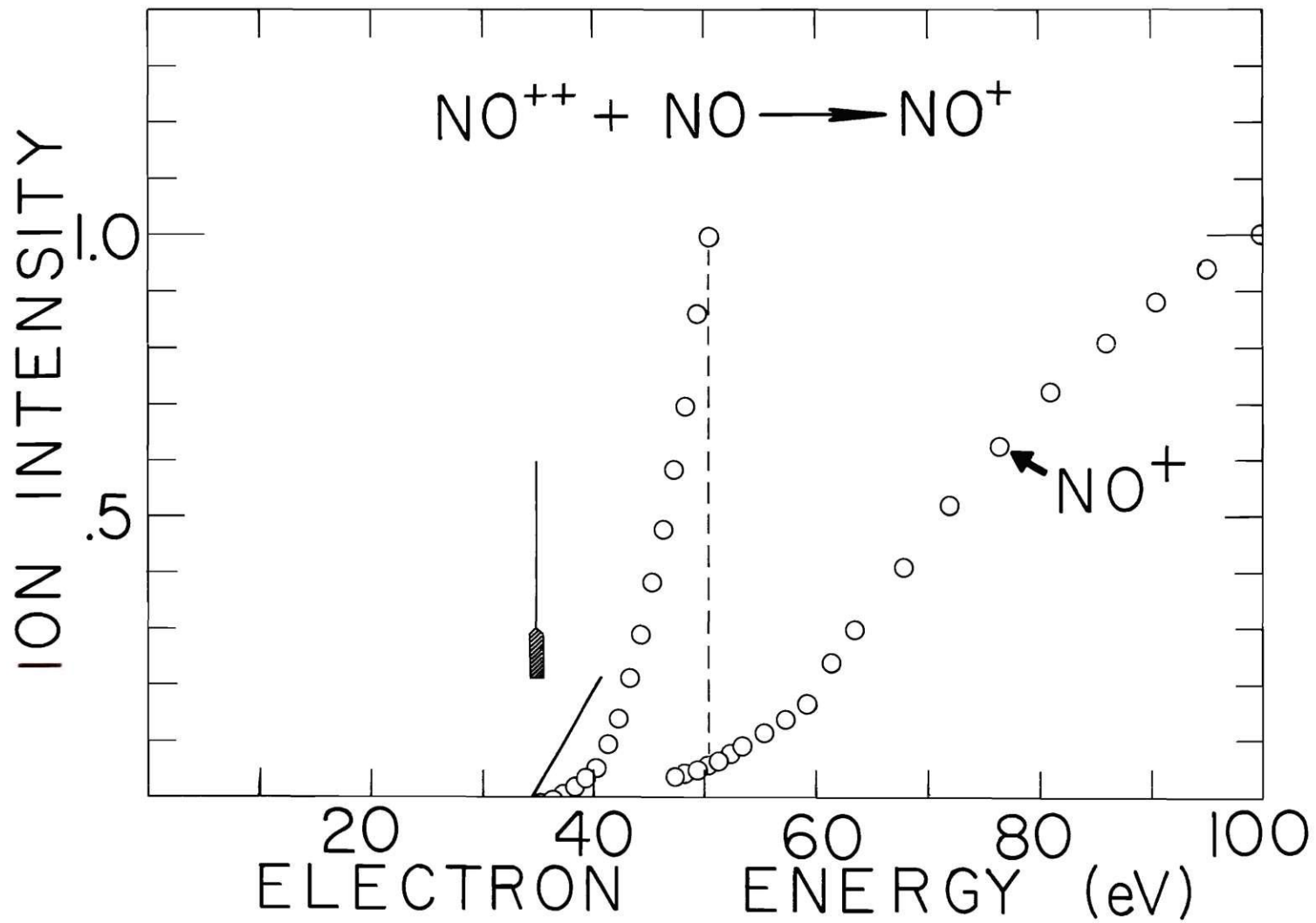


Figure 11. Ionization Efficiency Curve for  $\text{NO}^+$  Involved in the Reaction:  $\text{NO}^{++} + \text{NO} \rightarrow \text{NO}^+$ .

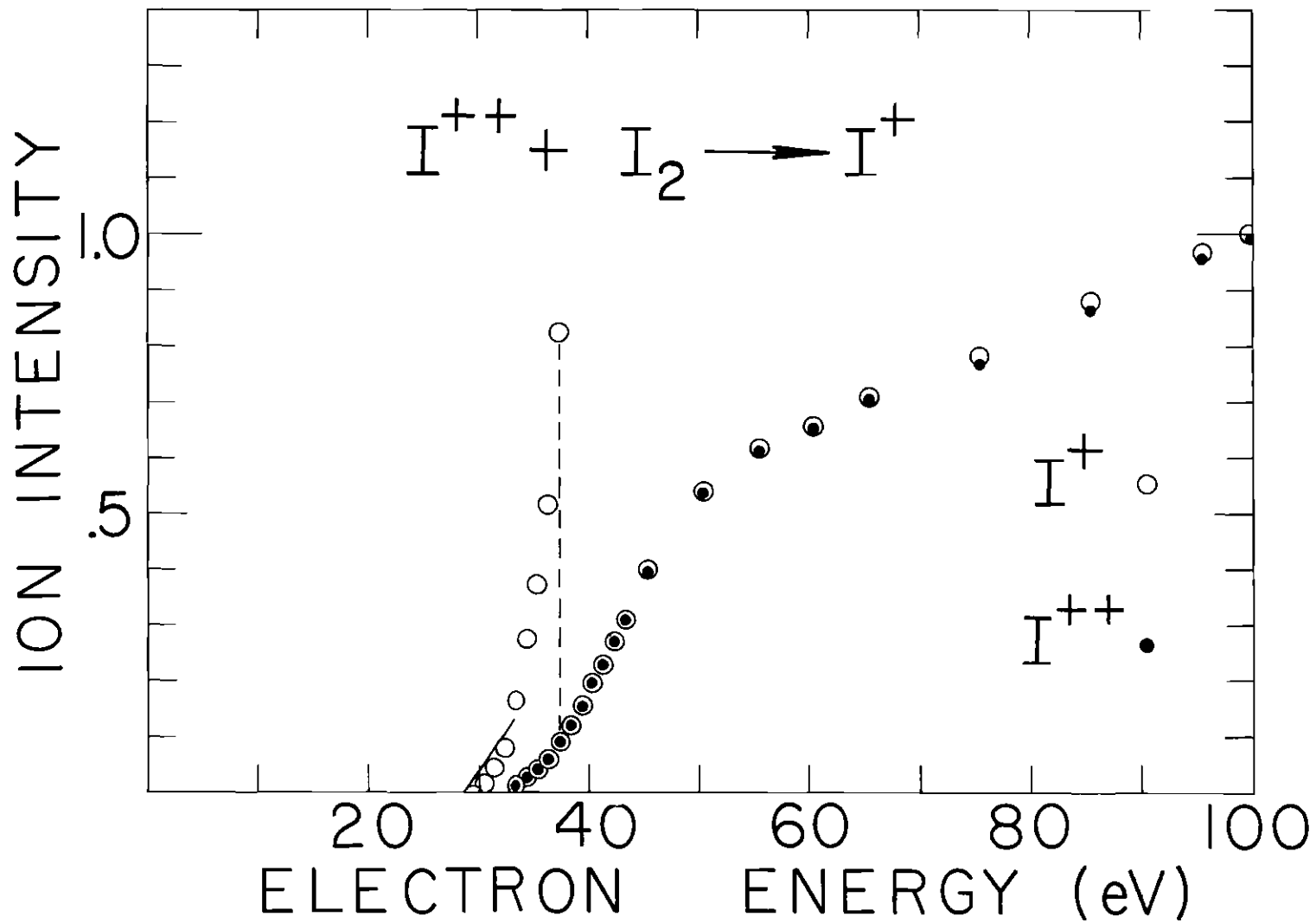


Figure 12. Ionization Efficiency Curves for Species Involved in the Reaction:  $I^{++} + I_2 \rightarrow I^+$ .

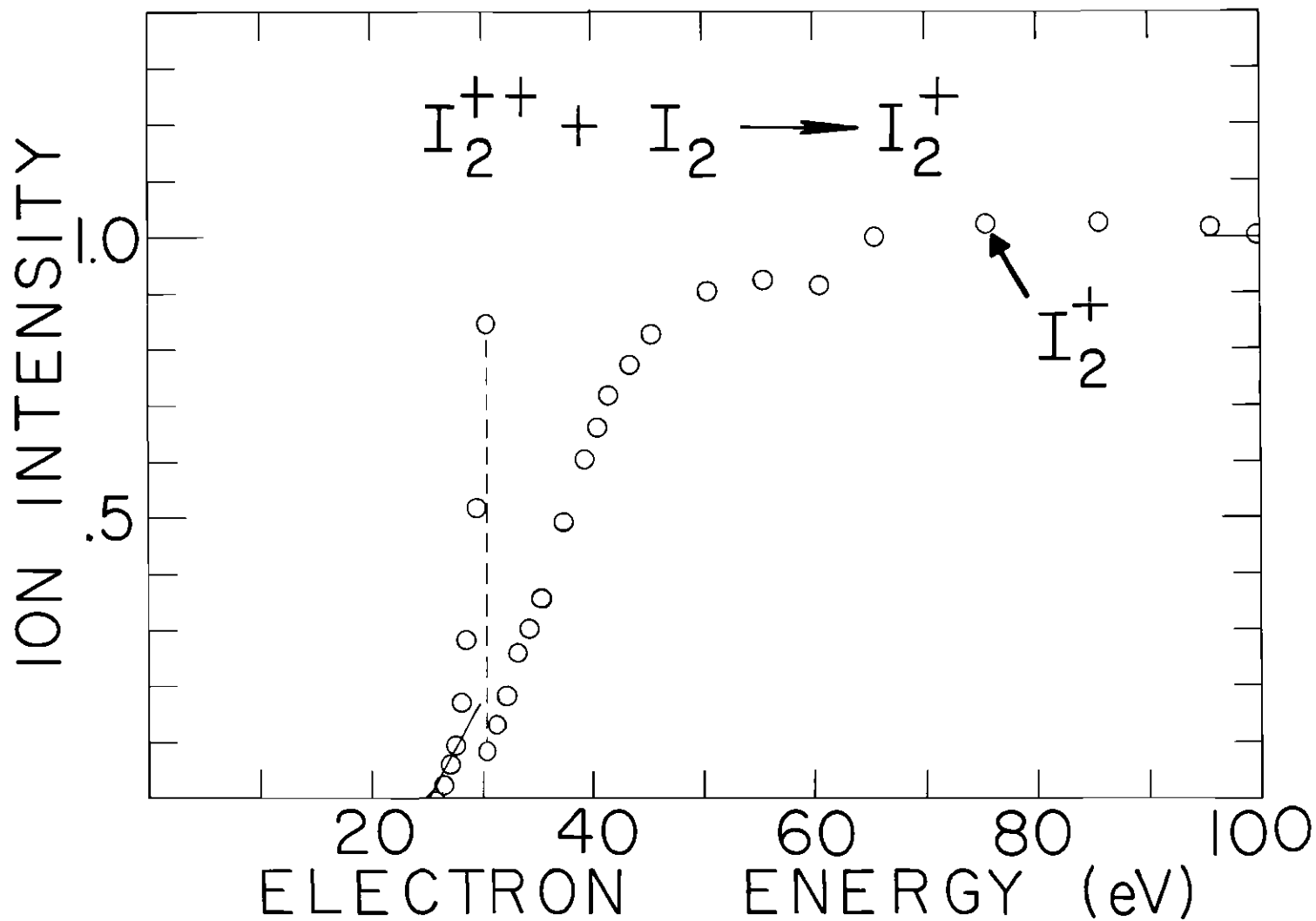


Figure 13. Ionization Efficiency Curve for  $I_2^+$  Involved in the Reaction:  $I_2^{++} + I_2 \rightarrow I_2^+$ .

Table 2. Appearance Potentials Obtained From Product Ion  
Efficiency Curves Analysis

Ion	Reaction	Appearance Potential
$\text{Ar}^{++}$	$\text{Ar}^{++} + \text{Ar} \rightarrow \text{Ar}^+$	43.2
$\text{N}_2^{++}$	$\text{N}_2^{++} + \text{Ar} \rightarrow \text{N}_2^+$	42.7
$\text{CO}^{++}$	$\text{CO}^{++} + \text{CO} \rightarrow \text{CO}^+$	41.7
$\text{O}_2^{++}$	$\text{O}_2^{++} + \text{Ar} \rightarrow \text{O}_2^+$	37.9 ± .1
$\text{CO}_2^{++}$	$\text{CO}_2^{++} + \text{CO}_2 \rightarrow \text{CO}_2^+$	37.0 ± .6
$\text{NO}^{++}$	$\text{NO}^{++} + \text{NO} \rightarrow \text{NO}^+$	35.3 ± .5
$\text{I}^{++}$	$\text{I}^{++} + \text{I}_2 \rightarrow \text{I}^+ + \text{I}_2^+$	29.0 ± 1
$\text{I}_2^{++}$	$\text{I}_2^{++} + \text{I}_2 \rightarrow \text{I}_2^+ + \text{I}_2$	25.2 ± .5

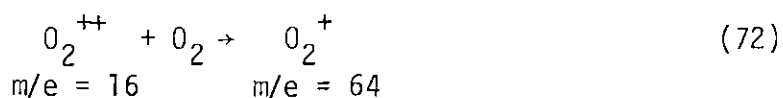
Table 3. Summary of Ground State Ionization Potentials for  $\text{CO}^{++}$ ,  $\text{N}_2^{++}$ ,  $\text{NO}^{++}$  and  $\text{O}_2^{++}$

	$\text{N}_2^{++}$	$\text{O}_2^{++}$	$\text{NO}^{++}$	$\text{CO}^{++}$
Present Results	42.7	$37.9 \pm .1$	$35.3 \pm .5$	41.7
Dorman et al. 1961 <sup>12</sup>			39.8	$41.8 \pm 0.3$
Dorman et al. 1963 <sup>13</sup>	$42.7 \pm 0.1$	$36.3 \pm 0.5$	--	--
Hurley 1962 (theoretical) <sup>14</sup>	42.63	35.48	38.1	$41.17-42.8$ <sup>20</sup>
Mark 1975 <sup>15</sup>	$42.9 \pm 0.3$	$35.6 \pm 0.3$	--	--
Moddeman et al. 1971 <sup>16</sup>	42.9	37.4	34.7 (O) 35.7 (N)	--
Siegbahn et al. 1969 <sup>17</sup>	42.7	--	--	--
Stalherm et al. 1969 <sup>18</sup>	43.3	--	--	--
Neuton et al. 1970 <sup>19</sup>	--	--	--	$41.5 \pm 0.4$

the literature value for the ionization potential of



$N_2^{++}$  ( $m/e = 14$ ) and  $O_2^{++}$  ( $m/e = 16$ ) ionization efficiency curves (found in Figure 7 and Figure 9 respectively) were obtained from the work of Mark.<sup>21</sup> Due to problems in detecting small magnitudes of the ion intensity associated with the  $O_2$  system, the ionization efficiency curve for



was extrapolated over a comparatively large energy range, as done by Mark. This is necessary since the Franck-Condon factors for the  $O_2^{++}(X^1\Sigma_g^+)$  states are small when  $v = 0,1,2,3,4$  and maximize at  $v = 6$ .

In all cases, ionization efficiency curves for the doubly charged reactants and for the singly charged product molecules were very similar. Therefore, one may conclude that in instances of high energy electron impact, the electronically excited states of doubly charged species that are produced react with equal probability. Relative energies computed for excited states of  $O_2^{++}$ ,  $N_2^{++}$  and  $NO^{++}$  are presented in Tables 4 through 6.

Table 4. Relative Energies of  $O_2^{++}$  Molecular Ion in eV

State	Hurley <sup>22</sup>
$X^1\Sigma_g^+$	0 <sup>†</sup>
$A^3\Sigma_u^+$	4.16
$B^3\Pi_g$	6.67
$B'^3\Sigma_u^-$	7.01
$a'^1\Sigma_u^-$	7.37
$\omega^1\Delta_u$	8.14
$a^1\Pi_g$	8.17
$C^3\Pi_u$	12.96

<sup>†</sup>These values correspond to the energy in the center of the Franck-Condon region.

Table 5. Relative Energies of  $N_2^{++}$  Molecular Ion in eV

State	Stalherm <sup>23</sup>	Hurley <sup>24</sup>
$X^1\Sigma_g^+$	0 +0.4 <sup>a</sup> -0.1	0 <sup>b</sup>
$X^3\Pi_u$	-0.1 +0.8 -0.4	-0.1
$A^3\Sigma_g^-$	1.0 +1.0 -0.6	1.04
$b^1\Pi_u$	1.3 +0.8 -0.5	1.26
$A^3\Pi_g$	3.5 +0.4 -0.2	3.41
$c^1\Pi$	5.9 +1.0 -0.6	5.91
$d^1\Sigma_u^+$	7.9 +0.4 -0.2	7.99

<sup>a</sup>Errors correspond to the Franck-Condon region on the potential energy curves.

<sup>b</sup>These values correspond to the energy at the center of the Franck-Condon region.

Table 6. Relative Energies of  $\text{NO}^{++}$  Molecular Ion in eV

State	Hurley <sup>25</sup>
$X^2_{\Sigma^+}$	0 <sup>†</sup>
$A^2_{\Pi}$	0.62
$B^2_{\Sigma^+}$	4.77

<sup>†</sup>These values correspond to the energy at the center of the Franck-Condon region.

## CHAPTER V

## WAVEFUNCTION OVERLAP

Transition Probability

A Born-Oppenheimer approximation may be used to estimate the vibrational population of different electronic states produced during ionization. The probability of a transition from vibrational level  $v'$  of the electronic state  $i$  of a diatomic molecule, to a vibrational level  $v''$  of the electronic state  $j$  is given by

$$P_{i v', j v''} \sim \left| \int \psi_{v'} R_{ij}^e (R, r) \psi_{v''} dR \right|^2, \quad (73)$$

For high energy electron impact the  $(V - V_v)$  term found in Equation (69) is approximately constant and the  $P_{i v', j v''}$  term will be dominated by the square of the overlap integrals. The electronic transition moment,  $R_{ij}^e (R, r)$ , is defined as

$$R_{ij}^e (R, r) = \int \psi_i \left( - \sum_s e r_s \right) \psi_j dT, \quad (74)$$

where  $\psi_i$  and  $\psi_j$  are the electronic wavefunctions for the states  $i$  and  $j$ , with electron coordinate vectors  $r_s$  fixed relative to the equilibrium internuclear distance  $R$ . The electronic dipole moment is given by  $\sum_s e r_s$ . One may assume  $R_{ij}^e (R, r)$  to be slowly varying over the range of internuclear distance  $R$  and the electron transition moment can be taken

outside the integral given in Equation (73). An alternate approximation for the variation of the electron transition moment with R has been examined by Fraser<sup>26</sup> who gives the transition probabilities as

$$P_{i v', j v''} \sim \{R_{ij}^e(\bar{R}_{v', v''})\}^2 \left| \int \psi_{v'} \psi_{v''} dR \right|^2, \quad (75)$$

where  $R_{ij}^e(\bar{R}_{v', v''})$  is termed the R centroid for transition. The  $R_{ij}^e(\bar{R}_{v', v''})$  term given above is much less dependent upon R, throughout a given band system, then the integral

$$\int \psi_{v'} \psi_{v''} dR. \quad (76)$$

Thus, the relative probabilities in moving from vibrational level  $v'$  in ionic state  $i$  of AB to vibrational level  $v''$  in ionic state  $j$  of  $AB^+$  will depend primarily upon the square of the vibrational overlap integral as was argued above. Vibrational wavefunctions describing the nuclear motion of a diatomic molecule moving under the influence of a Morse<sup>27</sup> potential are of the form

$$\psi_v = \{\alpha(K - 2v - 1)/\Gamma(K - v)v!\}^{1/2} e^{-Z/2} Z^{(K - 2v - 1)/2} \times (-1)^v L_v \quad (77)$$

with  $L_v$  a series

$$L_v = \{Z^v - v(K - v - 1)Z^{v-1} + v(v-1)(K - v - 1)(K - v - 2) \times (Z^{v-2}/Z!) + \dots + (-1)^v (K - v - 1)(K - v - 2)\dots(K - 2v)\} \quad (78)$$

which satisfies the recursion relation

$$L_v = Z L_{v-1} - (K - 2v) \sum_{r=0}^{v-1} \binom{v-1}{r} \frac{(2r)!}{(r+1)!} L_{v-r-1} \cdot \quad (79)$$

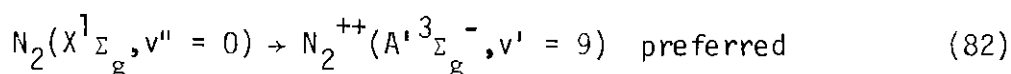
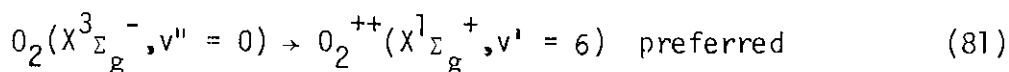
### Squares of Overlap Integrals

The vibrational wavefunctions presented above were used to calculate the squares of the overlap integrals for transitions of molecules from neutral to doubly charged excited states. In high energy electron impact it is probable that all excited states of the doubly charged species will be populated. Moreover, ionization efficiency curves for the double ionization are smooth curves which also match ionization efficiency curves for transitions from



This evidence implies that no one electronic state of  $AB^{++}$  is preferentially populated, or, all states are equally populated.

As seen from Tables 7 through 10, the  $AB^{++}$  formed in reaction has a wide range of probable vibrational levels. Transitions to a certain vibrational level,  $v' > 0$ , of an excited state are often preferred, as shown in the examples below:



The detailed vibrational distributions for the various electronic states of  $AB^{++}$  ions are presented in Tables 7 through 10.

Table 7. Squares of Overlap Integrals for the Ground  $N_2(X^1\Sigma_g^+, v'' = 0)$   
 State with Vibrational Levels  $v'$  of  $N_2^{++}$

$v'$	$N_2^{++}(X^3\Pi_u, v')$	$N_2^{++}(X^1\Sigma_g^+, v')$	$N_2^{++}(A^3\Sigma_g^-, v')$	$N_2^{++}(b^1\Pi_u, v')$	$N_2^{++}(A^3\Pi_g, v')$	$N_2^{++}(c^1\Pi_g, v')$	$N_2^{++}(d^1\Sigma_u^+, v')$
0	3.699 (-2)	5.164 (-1)	9.619 (-4)	2.008 (-2)	4.148 (-1)	2.123 (-1)	5.070 (-1)
1	1.034 (-1)	3.333 (-1)	5.053 (-3)	6.440 (-2)	5.852 (-1)	2.960 (-1)	3.388 (-1)
2	1.579 (-1)	1.156 (-1)	1.434 (-2)	1.129 (-1)		2.341 (-1)	1.193 (-1)
3	1.756 (-1)	2.831 (-2)	2.927 (-2)	1.438 (-1)		1.399 (-1)	2.890 (-2)
4	1.596 (-1)	5.416 (-3)	4.821 (-2)	1.495 (-1)		7.095 (-2)	5.248 (-3)
5	1.261 (-1)	8.406 (-4)	6.821 (-2)	1.352 (-1)		3.258 (-2)	7.182 (-4)
6	9.007 (-2)	1.055 (-4)	6.628 (-2)	1.105 (-1)		1.409 (-2)	
7	5.976 (-2)	1.006 (-5)	1.001 (-1)	8.384 (-2)			
8	3.752 (-2)	5.871 (-7)	1.087 (-1)	6.017 (-2)			
9	2.261 (-2)	4.870 (-9)	1.119 (-1)	4.144 (-2)			
10	1.323 (-2)	5.413 (-9)	1.103 (-1)	2.769 (-2)			

Table 8. Squares of Overlap Integrals for the Ground  $O_2(X^3\Sigma_g^-, v'' = 0)$   
 State with Vibrational Levels  $v'$  of  $O_2^{++}$

$v'$	$O_2^{++}(X^1\Sigma_g^+, v')$	$O_2^{++}(A^3\Sigma_u^+, v')$	$O_2^{++}(B^3\Pi_g, v')$	$O_2^{++}(B^3\Sigma_u^-, v')$	$O_2^{++}(a^1\Sigma_u^-, v')$	$O_2^{++}(w^1\Delta_u, v')$	$O_2^{++}(a^1\Pi_g, v')$	$O_2^{++}(C^3\Pi_u, v')$
0	1.459 (-4)	3.670 (-1)	7.366 (-1)	7.503 (-1)	8.190 (-1)	9.943 (-1)	8.557 (-1)	5.323 (-2)
1	1.827 (-3)	3.396 (-1)	2.571 (-1)	2.173 (-1)	1.667 (-1)	5.434 (-3)	1.429 (-1)	2.335 (-1)
2	1.055 (-2)	1.974 (-1)	4.854 (-3)	3.013 (-2)	1.390 (-2)	2.550 (-4)	2.844 (-4)	3.942 (-1)
3	3.726 (-2)	9.601 (-2)	1.464 (-3)	2.231 (-3)	3.387 (-4)	4.260 (-5)	1.044 (-3)	3.191 (-1)
4	8.986 (-2)		1.434 (-5)	4.735 (-5)	1.241 (-5)	1.298 (-6)	4.848 (-5)	
5	1.567 (-1)		2.505 (-5)	4.135 (-6)	1.919 (-5)	9.275 (-10)	3.764 (-6)	
6	2.039 (-1)		9.167 (-7)	5.530 (-6)	4.880 (-6)	3.425 (-9)	2.506 (-6)	
7	2.017 (-1)			1.705 (-6)	5.964 (-7)	7.085 (-10)	1.565 (-7)	
8	1.529 (-1)			2.913 (-7)	2.576 (-8)		2.928 (-9)	
9	8.887 (-2)			2.607 (-8)	8.407 (-10)		9.953 (-9)	
10	3.938 (-2)				3.481 (-9)		2.808 (-9)	

Table 9. Relative Franck-Condon Factors for  $\text{CO}^{++}(\chi^3_{\Pi, \nu''} = 0)$ 

$\nu'$	Franck-Condon Factor <sup>28</sup>
0	8.621 (-2)
1	2.020 (-1)
2	2.611 (-1)
3	2.512 (-1)
4	1.995 (-1)

Table 10. Squares of Overlap Integrals for the Ground  $\text{NO}(X^2\Pi, v'' = 0)$  State with Vibrational Levels  $v'$  of  $\text{NO}^{++}$

$v'$	$\text{NO}^{++}(X^2\Sigma^+, v')$	$\text{NO}^{++}(A^2\Pi, v')$	$\text{NO}^{++}(B^2\Sigma^+, v')$
0	3.639 (-1)	9.936 (-1)	2.538 (-1)
1	4.272 (-1)	4.994 (-3)	4.572 (-1)
2	1.760 (-1)	1.208 (-3)	2.490 (-1)
3	3.001 (-2)	1.611 (-4)	3.938 (-2)
4	1.810 (-3)	1.863 (-6)	3.551 (-4)
5	1.307 (-5)	2.915 (-7)	2.228 (-4)
6	8.299 (-7)	1.166 (-7)	3.770 (-6)
7	2.088 (-8)	9.987 (-9)	3.571 (-6)
8	1.941 (-9)	1.438 (-10)	2.237 (-8)
9	4.287 (-12)	3.026 (-11)	4.814 (-8)
10	7.249 (-12)	2.230 (-11)	1.172 (-8)

## CHAPTER VI

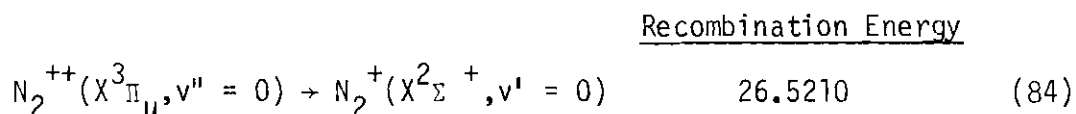
## RECOMBINATION ENERGY

Reactions of the type



possess a characteristic change in energy designated by  $\Delta E_{\text{reaction}}$ .

The value of  $\Delta E_{\text{reaction}}$  varies with the electronic states of the species involved and with the vibrational level of the species. Transitions from  $\text{N}_2^{++}(\text{X}^3\Pi_u, v'' = 0)$  to excited states of  $\text{N}_2^+$  have a  $\Delta E_{\text{reaction}}$  given below:



Although this chart includes only transitions between the 0<sup>th</sup> vibrational levels of  $\text{N}_2^{++}$  and  $\text{N}_2^+$ , transitions between the zero vibrational levels do not always have the highest probability of occurring. The probability of a particular transition



will depend upon the vibrational overlap term and upon the initial population of the  $N_2^{++}(v'')$  state.

Figures 14 and 15 show the relative probability of the  $N_2^{++}$  ion having a particular recombination energy, R.E., due to transitions from  $N_2^{++}$  to  $N_2^+$ . If all states of  $N_2^{++}$  are equally populated then the resultant R.E.s for the production of  $N_2^+$  would be an equally weighted average of all the R.E.s from the individual  $N_2^{++}$  states. Maximum occurrence of particular values for the R.E. exist and can be identified from Figure 16. R.E.s which are heavily populated include ranges from 17.4-19.7 eV, from 22.2-23.3 eV, and from 24.3-27.4 eV.

As seen from Equation (83), the production of  $N_2^+$  from  $N_2^{++}$  is accompanied by the ionization of AB to  $AB^+$ . When the ionization potential, I.P., of AB is approximately equal to the R.E.  $N_2^{++} \rightarrow N_2^+$  the  $\Delta E_{\text{reaction}}$  will be small. Small values of  $\Delta E_{\text{reaction}}$  imply that the overlap between the states of the reaction molecules is good, or, the reaction cross section is large.

Dissociation asymptotes, drawn in on Figure 16, represent only the minimum energy value for each dissociation curve. Precise energy values at which the dissociation curve crosses the Franck-Condon region are unknown.

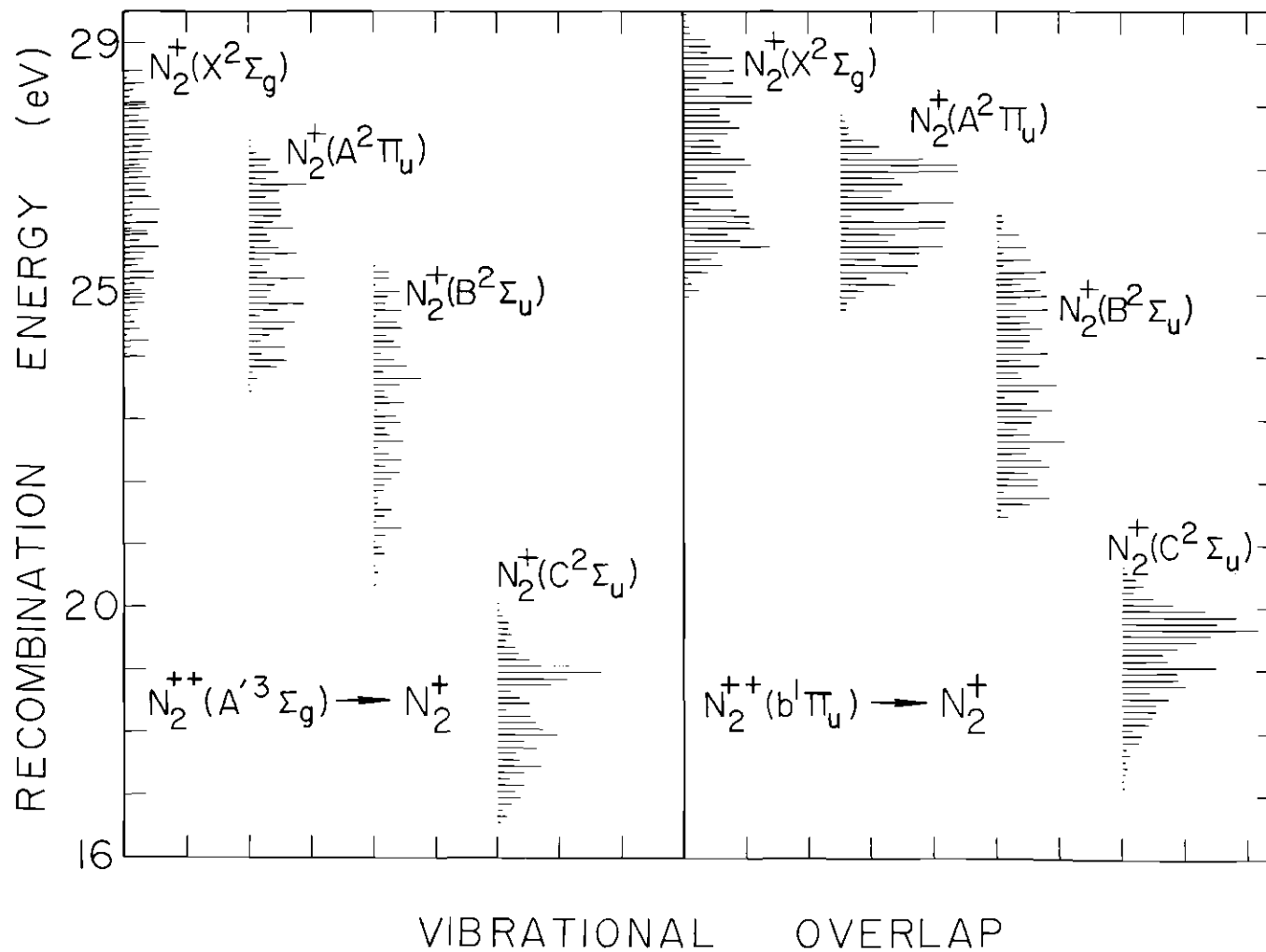


Figure 14. Graphs of the Relative Probability for Transitions from  $N_2^{++}$

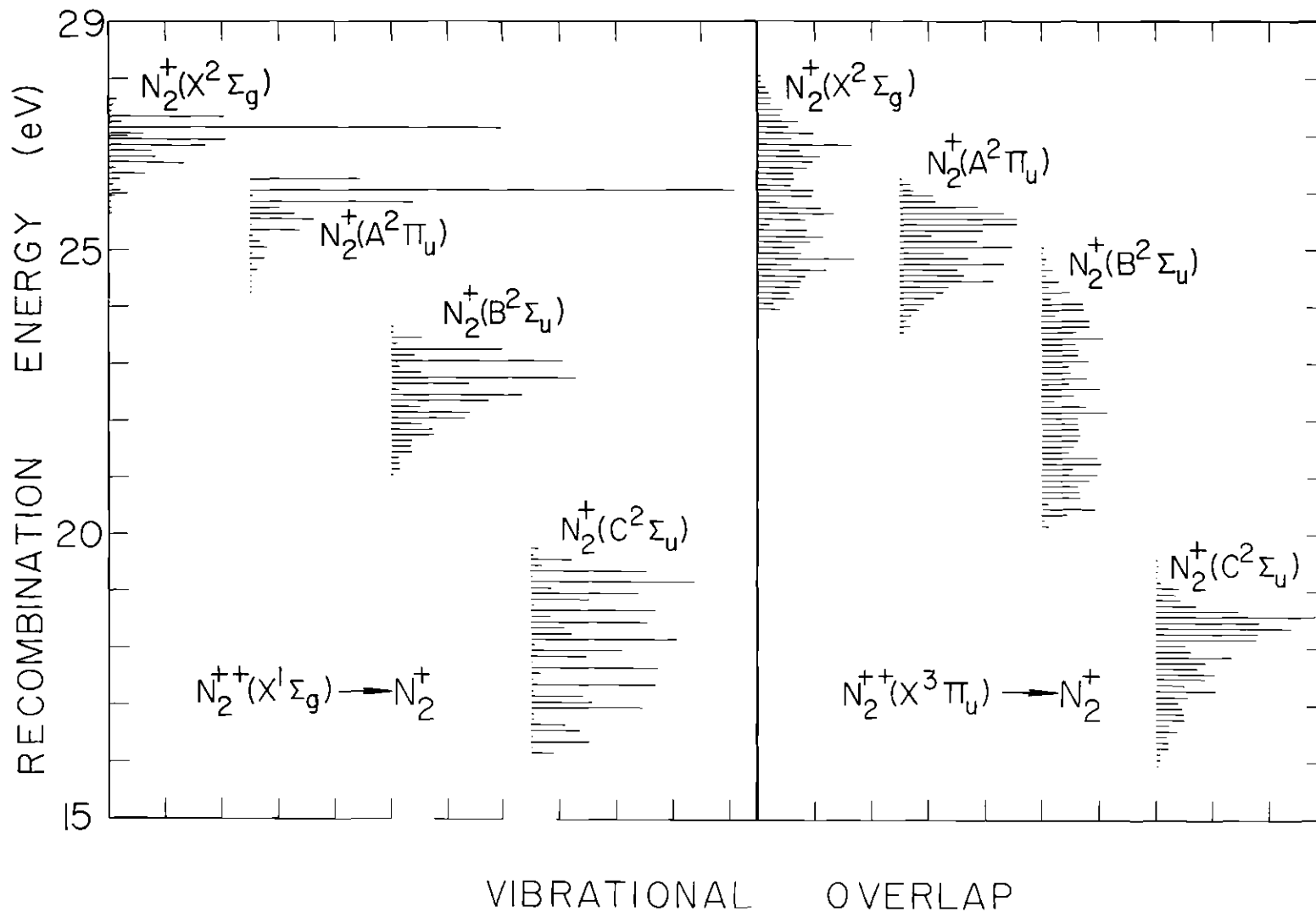


Figure 15. Relative Probability of Transitions from  $N_2^{++}(X^1\Sigma_g^+)$  and  $X^3\Pi_u)$

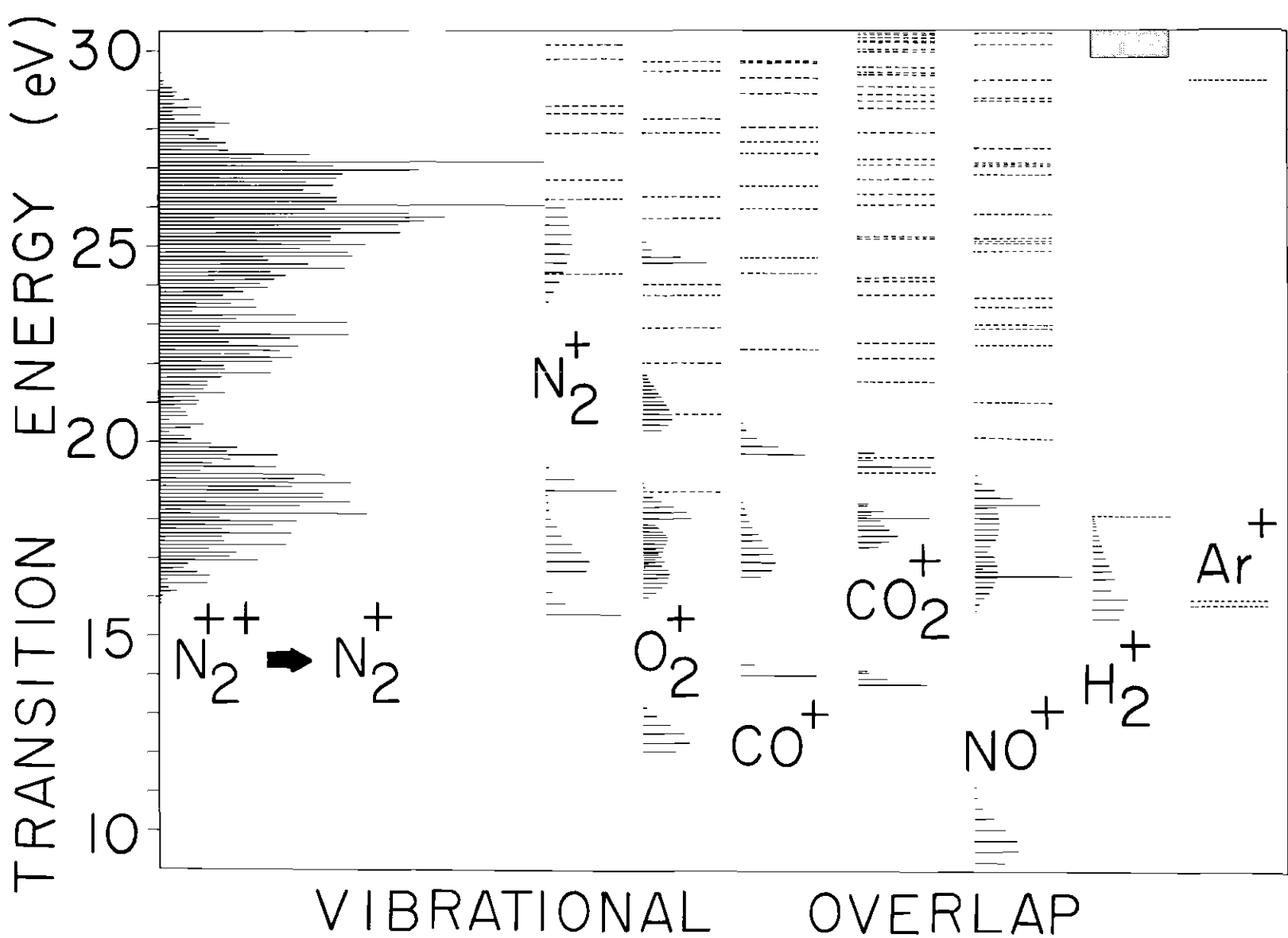


Figure 16. Recombination Energy  $N_2^{++}$  Averaged

## CHAPTER VII

## REACTION CROSS SECTIONS

Calculations

The flux of  $N_2^+$  products from the reaction



is expressed as

$$i_{N_2^+ \text{ product}} = i_{N_2^{++} - N_2} \sigma_{N_2^{++} - N_2} n \ell . \quad (90)$$

Similarly, the flux of  $N^0$  products from the reaction



is expressed as

$$i_{N^0} = i_{N^+ - N_2} \sigma_{N^+ - N_2} n \ell . \quad (92)$$

Taking the ratios of these two values one obtains:

$$i_{N_2^+ \text{ prod}} / i_{N^0} = i_{N_2^{++} - N_2} \sigma_{N_2^{++} - N_2} n \ell / i_{N^+ - N_2} \sigma_{N^+ - N_2} n \ell . \quad (93)$$

Solving the expression above for the cross section for the reaction of  $N_2^{++} + N_2$  produces

$$\sigma_{N_2^{++}-N_2} = (i_{N_2^+} / i_{N^0}) (i_{N^+} / i_{N_2^{++}}) \sigma_{N^+-N_2} . \quad (94)$$

From the work of T.D. Marc,<sup>29</sup> it has been determined that

$$(i_{N^+} / i_{N_2^{++}}) = 1/.0645 . \quad (95)$$

In addition, the ratio of  $i_{N_2^+ \text{ product}}$  to  $i_{N^0}$  can be set equal to

$$i_{N_2^+ \text{ product}} / i_{N^0} = (\text{peak height } N_2^+ \text{ product}) \gamma_{N_2^+}^{-1} / (\text{peak height } N^0) \gamma_{N^0}^{-1} \quad (96)$$

where  $\gamma$  is the secondary electron emission coefficient for the electron multiplier. Since  $N_2^+ \text{ product}$  has a kinetic energy equal to twice that of  $N^0$ , the velocities of these two ions will be equivalent by virtue of the fact

$$KE = \frac{1}{2}mv^2 . \quad (97)$$

However, the secondary emission coefficient of  $N_2^+$  has been determined to be twice that of  $N^0$ , at the same velocity, in agreement with work done by L.N. Large.<sup>30</sup> Using Equation (94), absolute cross sections have been determined and presented in Table 11.

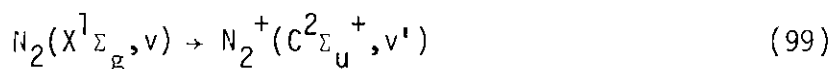
Table 11. Cross Sections in the Range 1000-3000 eV for Reactions  
of the Type  $N_2^{++} + AB \rightarrow N_2^+ + AB^+$

	Q ( $\text{\AA}$ ) <sup>2</sup>			
	AB = N <sub>2</sub>	O <sub>2</sub>	CO <sub>2</sub>	CO
3000	43	20.2	22.4	17.8
2000	49	16.1	25.5	24.3
1000	60	13.0	41.6	28.3

Considering the spread of recombination energies produced via transitions from excited states of  $N_2^{++}$  to excited states of  $N_2^+$ , it is obvious why collision reactions of the form

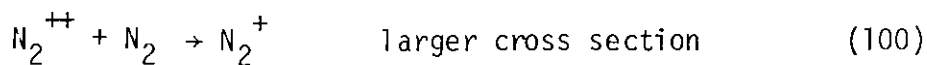


have large cross sections. There are a relatively large number of  $N_2^{++}$  ions which can provide a recombination energy equal to the I.P. required to promote  $N_2$  to all excited states of  $N_2^+$ , except  $C^2\Sigma_u^+$ . Despite an apparently adequate number of  $N_2^{++}$  ions with a R.E. sufficient to produce a transition from



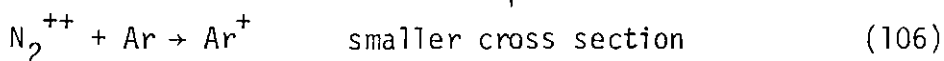
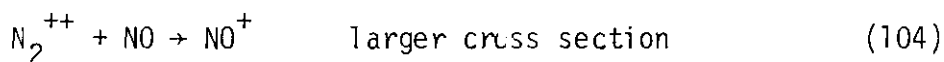
this particular state of  $N_2^+$  is subject to predissociation.<sup>31,32,33</sup>

Similar arguments may be used to explain the cross section measurements of reactions between  $N_2^{++}$  and other molecules presented in Table 11. These time-of-flight determinations of cross sections between  $N_2^{++}$  and various diatomic molecules produces the following ordering based upon the relative magnitude of each reaction's cross section:



The reasons for such a small cross section in the reaction of  $N_2^{++}$  with  $O_2$  is evident. Overlap between the R.E.  $N_2^{++} \rightarrow N_2^+$  and the I.P.  $O_2 \rightarrow O_2^+$  is not adequate to produce a large cross section. Even at energy levels where there exists an overlap of R.E. and I.P., the number of  $N_2^{++}$  ions capable of yielding that particular R.E. is a low percentage of the total population. With regard to  $CO_2$  and  $CO$ , the amount of overlap between R.E.  $N_2^{++} \rightarrow N_2^+$  and the I.P. of these molecules is great enough to produce larger cross sections than the reaction of  $N_2^{++}$  with  $O_2$ .

Studies of the overlap between R.E.  $N_2^{++} \rightarrow N_2^+$  and I.P. of other molecules allows one to predict the relative magnitude of reaction cross sections. In particular, the following rank of reactions, with respect to their cross sections, would be expected.



Good overlap exists between R.E.  $N_2^{++} \rightarrow N_2^+$  and the I.P. of most of the excited states of  $NO^+(b^3\Pi, a^3, w^3\Delta \text{ and } A^1\Pi)$ ; however, overlap with  $NO^+(X^1\Sigma)$  is non-existent. With  $H_2$  one finds overlap in only the higher vibrational levels of  $H_2^+(X^2\Sigma_g)$ . Finally, in the case of  $Ar$ , overlap of any type is very small.

## CHAPTER VIII

## CONCLUSIONS

Ionization efficiency curves for doubly charged ions have been determined using a double focusing, magnetic mass spectrometer. The shape of the ionization efficiency curves for the  $AB^+$  product are the same as the ionization efficiency curves determined for  $AB^{++}$ . This indicates that all populated, excited states of  $AB^{++}$  reactants have approximately the same charge transfer cross section. Franck-Condon factors have been computed for the  $N_2 \rightarrow N_2^{++}$  system using Morse anharmonic wavefunctions. From these factors, the vibrational state distribution of  $N_2^{++}$  ions in these experiments has been determined in the cases of ions occupying the lowest three electronically excited states. It has been shown that the doubly charged reactant ions are formed over a range of levels and that the 0<sup>th</sup> vibrational level is not necessarily preferred. Figures 14 and 15 of this thesis show the relative distribution of recombination energies for transitions from each excited state of  $N_2^{++}$  to each excited state of  $N_2^+$ . The range of recombination energies for all transitions from  $N_2^{++}$  to  $N_2^+$  are compiled in Figure 16. It is found that the recombination energies of  $N_2^{++}$  occur with high probability in the intervals 24.3-27.4 eV, 22.2-23.3 eV and 17.4-19.7 eV; however, the actual span of possible recombination energies is from 15.8-29.6 eV. Thus, for reactions of the form



the cross section of reaction will depend upon the overlap between the energy released in the  $N_2^{++} \rightarrow N_2^+$  process and the energy required for ionization of AB in  $AB \rightarrow AB^+$ . Reactants AB which have good overlap between their excited states of  $AB^+$  and the recombination energy for  $N_2^{++} \rightarrow N_2^+$  (Figure 18) have a large charge transfer cross section. Those reactant systems that have large energy defects and small overlaps with the product system have a small probability for charge transfer with  $N_2^{++}$ .

## LITERATURE CITED

1. J.D. Craggs and H.S.W. Massey, Encyclopedia of Physics (editor, S. Flügge), Vol. XXXVII, Heidelberg, W. Germany: Springer Verlag, 1959.
2. G.L. Weissler, Encyclopedia of Physics (editor, S. Flügge), Vol. XXI, Heidelberg, W. Germany: Springer Verlag, 1959.
3. M.I. Jaboury and D.W. Turner, J. Chem. Soc. 7, 5141 (1963).
4. A.C. Hurley and V.W. Maslen, J. Chem. Phys. 34, 1919 (1961).
5. C.A. McDowell, "The Ionization and Dissociation of Molecules", Mass Spectrometry, (editor, C.A. McDowell), New York, New York: McGraw Hill, 1963.
6. F.H. Dorman, J.D. Morrison and A.J.C. Nicholson, J. Chem. Phys. 31, 1335 (1959).
7. J.D. Morrison and A.J.C. Nicholson, J. Chem. Phys. 31, 1320 (1959).
8. F.H. Dorman and J.D. Morrison, J. Chem. Phys. 35, 575 (1961).
9. Sydney Geltman, Physical Review 102, 171 (1956).
10. G.H. Wannier, Physical Review 100, 1180 (1955).
11. A.S. Coolidge, H.M. James and R.D. Present, J. Chem. Phys. 4, 193 (1936).
12. F.H. Dorman and J.D. Morrison, J. Chem. Phys. 35, 575 (1961).
13. F.H. Dorman and J.D. Morrison, J. Chem. Phys. 39, 1906 (1963).
14. A.C. Hurley, J. Mol. Spectrosc. 9, 18 (1962).
15. T.D. Märk, J. Chem. Phys. 63, 3731 (1975).
16. W. Moddeman, T. Carlson, M. Krause and B. Pullen, J. Chem. Phys. 55, 2317 (1971).
17. K. Siegbahn et al., ESCA Applied to Free Molecules (1969).
18. D. Stalherm, B. Cleff, H. Hillig and W. Melhorn, Z. Naturforsch. 24a, 1728 (1969).

19. A. Newton and A. Sciamanna, J. Chem. Phys. 53, 132 (1970).
20. A.C. Hurley and V.W. Maslen, J. Chem. Phys. 34, 1919 (1961).
21. T.D. Märk, J. Chem. Phys. 63, 3731 (1975).
22. A.C. Hurley, J. Mol. Spectrosc. 9, 18 (1962).
23. D. Stalherm, B. Cleff, H. Hillig and W. Melhorn, Z. Naturforsch. 24a, 1728 (1969).
24. A.C. Hurley, J. Mol. Spectrosc. 9, 18 (1962).
25. A.C. Hurley, J. Mol. Spectrosc. 9, 18 (1962).
26. P.A. Fraser, Can. J. Phys. 32, 515 (1954).
27. P.M. Morse, Phys. Rev. 34, 57 (1929).
28. R.G. Hirsch, R.J. Van Brunt and W.D. Whitehead, Int. J. of Mass Spectrometry and Ion Physics 17, 335 (1975).
29. T.D. Märk, J. Chem. Phys. 63, 3731 (1975).
30. L.N. Large, Proc. Phys. Soc. 81, 1101 (1963).
31. J.C. Lorquet and M. Desouter, Chem. Phys. Lett. 16, 136 (1972).
32. J. Tellinghuisen and D.L. Albritton, Chem. Phys. Lett. 31, 91 (1975).
33. A.L. Roche and H. Lefebvre-Brion, Chem. Phys. Lett. 32, 155 (1975).